The Journal of Chemical Physics

RESEARCH ARTICLE | APRIL 07 2025

# Homogeneous nucleation rate of carbon dioxide hydrate formation under experimental condition from Seeding simulations

I. M. Zerón ; J. Algaba ; J. M. Míguez ; J. Grabowska ; S. Blazquez ; E. Sanz ; C. Vega ; F. J. Blas



*J. Chem. Phys.* 162, 134708 (2025)
https://doi.org/10.1063/5.0252152

The Journal of Chemical Physics ARTICLE pubs.aip.org/aip/jcp

# Homogeneous nucleation rate of carbon dioxide hydrate formation under experimental condition from Seeding simulations

Cite as: J. Chem. Phys. 162, 134708 (2025); doi: 10.1063/5.0252152
Submitted: 7 December 2024 • Accepted: 16 March 2025 •
Published Online: 7 April 2025



I. M. Zerón,[1] J. Algaba,[1] J. M. Míguez,[1] J. Grabowska,[2] S. Blazquez,[3] E. Sanz,[3] C. Vega,[3] and F. J. Blas[1,a)]

## AFFILIATIONS

[1] Laboratorio de Simulación Molecular y Química Computacional, CIQSO-Centro de Investigación en Química Sostenible and Departamento de Ciencias Integradas, Universidad de Huelva, 21006 Huelva, Spain
[2] Department of Physical Chemistry, Faculty of Chemistry, Gdansk University of Technology, ul. Narutowicza 11/12, 80-233 Gdansk, Poland
[3] Dpto. Química Física, Fac. Ciencias Químicas, Universidad Complutense de Madrid, 28040 Madrid, Spain

[a)] **Author to whom correspondence should be addressed:** felipe@uhu.es



## ABSTRACT

We investigate the nucleation of carbon dioxide ($CO_2$) hydrates from carbon dioxide aqueous solutions by means of molecular dynamics simulations using the TIP4P/Ice and the TraPPE models for water and $CO_2$, respectively. We work at 400 bar and different temperatures and $CO_2$ concentrations. We use brute force molecular dynamics when the supersaturation or the supercooling is so high so that nucleation occurs spontaneously and Seeding otherwise. We use both methods for a particular state and found an excellent agreement when using a linear combination of $\overline{q}_3$ and $\overline{q}_{12}$ order parameters to identify critical clusters. With such order parameter, we get a rate of $10^{25}$ m$^{-3}$ s$^{-1}$ for nucleation in a $CO_2$ saturated solution at 255 K (35 K of supercooling). By comparison with our previous work on methane hydrates, we conclude that nucleation of $CO_2$ hydrates is several orders of magnitude faster due to a lower interfacial free energy between the crystal and the solution. By combining our nucleation studies with a recent calculation of the hydrate–solution interfacial free energy at coexistence [Algaba *et al.*, J. Colloid Interface Sci. **623**, 354–367 (2022)], we obtain a prediction of the nucleation rate temperature dependence for $CO_2$-saturated solutions (the experimentally relevant concentration). On the one hand, we open the window for comparison with experiments for supercooling larger than 25 K. On the other hand, we conclude that homogeneous nucleation is impossible for supercooling lower than 20 K. Therefore, nucleation must be heterogeneous in typical experiments where hydrate formation is observed at low supercooling. To assess the hypothesis that nucleation occurs at the solution-$CO_2$ interface, we run spontaneous nucleation simulations in two-phase systems and find, by comparison with single-phase simulations, that the interface does not affect hydrate nucleation, at least at the deep supercooling at which this study was carried out (40 and 45 K). Overall, our work sheds light on molecular and thermodynamic aspects of hydrate nucleation.



## I. INTRODUCTION

When a liquid is cooled below the solid–liquid coexistence temperature, the crystallization is not an immediate process and the liquid can remain in a metastable supercooled state for some time. Fluctuations still exist and the formation of small embryos of the stable crystal phase can be observed. When these fluctuations lead to the formation of a solid cluster that surpasses a critical size then crystallization cannot be avoided. This mechanism is usually known as homogeneous nucleation. In the proximity of the equilibrium freezing temperature, the critical cluster size is quite large and the liquid phase can remain stable for quite a long time. The presence of solid impurities reduces the size of the critical cluster and makes nucleation easier, leading to heterogeneous nucleation that can be

observed easily even for temperatures moderately below the freezing temperature.[1]

An interesting observable is the nucleation rate $J$ defined as the number of critical clusters per unit of time and volume. The nucleation rate can be determined in experiments, mainly for ice in supercooled water[2–11] but only (due to limitations in system size and accessible time) when its value is smaller than $10^{16}/(\mathrm{m}^3\ \mathrm{s})$. In simulations, the nucleation rate can be determined in Brute Force (BF) simulations only when its value is of the order of $10^{30}/(\mathrm{m}^3\ \mathrm{s})$ or higher (due to limitations in system size and accessible time). Thus, there is a range of nucleation rates between $10^{16}$ and $10^{30}/(\mathrm{m}^3\ \mathrm{s})$ that cannot be accessed either by experiments or by BF simulations. However, the use of special rare event technique simulations allows determining the nucleation rate in this intermediate regime or even for temperatures accessible in experiments.

Several techniques have been proposed to obtain nucleation rates in simulations when BF simulations are not sufficient. Two of them, Umbrella Sampling[12] (US) and Metadynamics,[13] are aimed at determining the free energy barrier for nucleation and the nucleation rate using the formalism proposed by Volmer and Weber[14] and Becker and Döring.[15] About 25 years ago, Bolhuis and coworkers proposed a methodology, the Transition Path Sampling (TPS),[16] where an analysis of the trajectories that are reactive (i.e., leading from the metastable phase to the stable phase) is performed, allowing the determination of nucleation rates. About twenty years ago, another method, the Forward Flux Sampling (FFS),[17,18] was proposed to analyze the fraction of successful trajectories leading from one value of the order parameter to the next and the flux to the initial lowest order value of the order parameter considered. The nucleation rates obtained by these four methods (umbrella sampling, metadynamics, transition path sampling, and forward flux sampling) are, in principle, exact (or almost exact) for the considered potential model.

More recently, some of us[19] and independently Knott *et al.*[20] introduced a new approximate technique to determine nucleation rates known as Seeding. In this technique, a solid cluster is inserted into a metastable fluid and the conditions under which this cluster is critical (i.e., with 50% probability of evolving to either phase) are determined. This followed the first ideas about using seeds for nucleation studies introduced by Bai and Li.[21,22] Once the size of the critical cluster is determined then the expression of the Classical Nucleation Theory (CNT) is used to estimate the nucleation rate. The main disadvantage of Seeding is that it is an approximate technique as the results depend on the choice of the order parameter. However, its main advantage is its simplicity thus, allowing studying really complex systems for which more rigorous methods are too expensive from a computational point of view. It has been shown, that with appropriate order parameters, Seeding correctly predicts the nucleation rates of hard spheres, Lennard-Jones systems,[23] electrolytes,[24] or even the nucleation of ice from both pure water and aqueous electrolyte solutions.[25,26] Recently, we have shown that it can also predict the nucleation rate of hydrate formation for methane hydrate.[27]

Hydrates are non-stoichiometric solids formed when a gas (typically methane or carbon dioxide) is in contact with water under moderate pressure (i.e., 30–1000 bar) and the system is cooled. In the most common hydrate structure (sI), the unit cell has cubic symmetry and contains 46 molecules of water and 8 molecules of guest (occupying two types of cavities, six large and two somewhat smaller).[28–30] Methane hydrates can be found naturally on the seafloor near coasts and it is also formed in the pipes transporting natural gas.[31] It is also expected to be found on some planets.[32] Although methane hydrate is the most relevant, the interest in hydrate containing carbon dioxide ($CO_2$) is growing. This is so because replacing methane by $CO_2$ in the hydrate would be a simple procedure to sequestrate $CO_2$ from the atmosphere and to mitigate its greenhouse effect that leads to global warming.[33,34]

When the gas is in contact with water, the formation of the hydrate starts at a certain temperature denoted as $T_3$.[28] This temperature is indeed a triple point, where three phases, the solid hydrate, the aqueous solution, and the gas, coexist at equilibrium. The value of $T_3$ depends on the pressure, and nucleation rates increase dramatically as one moves from $T_3$ to lower temperatures at constant pressure.

Several experimental studies deal with hydrate nucleation.[35–42] Many computational studies on hydrate nucleation have also been reported.[17,20,30,43–66] Comparison between experimental and simulation studies is difficult due to the presence of heterogeneous nucleation in experiments and the fact that in many simulation studies, one must use large supersaturations (i.e., solubilities of the gas artificially higher than the experimental ones) to increase the driving force to facilitate the kinetics of the nucleation process. In their pioneering molecular dynamics (MD) study, Walsh *et al.*[47] used a high concentration of methane in the aqueous solution in order to observe nucleation events in a reasonable simulation time. In fact, using a supersaturated solution of the guest molecule is a common strategy in the studies of nucleation of hydrates. There are two ways to prepare such a system. The first one is to use a homogeneous solution of guest molecule in water,[50,51] in which the concentration of solute is higher than the equilibrium solubility under the same conditions. However, this is only possible at low temperatures, where the nucleation of the hydrate is faster than the nucleation of gas bubbles.[67] The second option is to use a system in which there is a curved interface between the solution and the gas phase[47,56–58] (i.e., bubbles of gas in the solution). The presence of a curved interface results in an increase in the solubility of the guest molecule in water. These two methods allow obtaining spontaneous nucleation events in BF simulations.[47,50,51] In addition, Arjun *et al.*[56–58] were able to estimate the nucleation rate of hydrates at temperatures well below $T_3$ by combining transition path sampling with the use of gas bubbles, which increases the solubility of the gas. In experiments, however, the concentration of guest molecules in the solution is dictated by the equilibrium solubility of the solute in water via a planar interface. For that reason, in this work, we study the nucleation of hydrate under experimental conditions, i.e., we use the concentration of guest molecule ($CO_2$ in this work) equal to its equilibrium solubility. To the best of our knowledge, there are only two simulation studies where the nucleation rate was computed under "realistic experimental conditions" (without supersaturation) for the formation of the methane hydrate. In the first one, Arjun and Bolhuis[59] in a tour de force used TPS to determine the nucleation rate. In the second one, we used the Seeding technique.[27] Good agreement was found between the estimates of the nucleation rate from these two studies.

In this work, we shall use the Seeding technique[23] to determine by computer simulations the homogeneous nucleation rate of the $CO_2$ hydrate at the pressure of 400 bar and when the supercooling $\Delta T = T_3 - T$, (i.e., the difference between the dissociation temperature $T_3$ and the current temperature $T$) is equal to 35 K. We shall determine the nucleation rate under experimental conditions (i.e., without supersaturation). This study is a follow-up of a previous study where we used the same technique to study the nucleation rate of methane hydrate at the same pressure and degree of supercooling.[27] The comparison will be useful as it illustrates the differences in the nucleation rate of hydrates of methane and $CO_2$ under the same thermodynamic conditions (i.e., equal pressure and degree of supercooling). At first, one would expect that the differences between both gases should not be too large as the guest molecules are of similar size. However, the solubility of $CO_2$ in water is an order of magnitude larger than that of methane (due to its large quadrupole moment leading to more favorable water–gas interactions). It will be shown that the nucleation rate of the $CO_2$ hydrate is much higher for a certain fixed pressure and a certain fixed supercooling compared to methane hydrate. The comparison is especially useful as we are using the same water model that was employed in our previous study of methane, namely, TIP4P/Ice. Although the higher nucleation rate for the $CO_2$ hydrate may be due to its higher solubility,[68] we think the main reason for this is the lower value of the interfacial free energy between the hydrate and the aqueous solution.

Finally, we shall analyze the impact of the gas–water interface on the nucleation rate. Hydrates are always obtained in experiments by considering a two-phase system (gas in contact with water). There is the possibility that the presence of the interface facilitates the nucleation of the solid phase. Thus, heterogeneous nucleation (due to the presence of the gas–water interface rather than the presence of solid impurities in the liquid phase) may be responsible for the nucleation found in experiments. To determine this point, we performed simulations both in the presence and in the absence of the interface with the same concentration of $CO_2$ in the aqueous solution. We conclude that nucleation rates obtained in both cases were the same, suggesting that the gas–water interface does not enhance the nucleation rate, at least for the thermodynamic conditions considered in this work.

The organization of this paper is as follows: in Sec. II, we describe the methodology used in this work. The results obtained, as well as their discussion, are described in Sec. III. Finally, conclusions are presented in Sec. IV.

## II. METHODOLOGY

### A. Seeding: A brief description

From the description of the CNT,[14,15,69,70] the formation of a solid cluster of size $N$ at given temperature $T$ and pressure $P$ into the liquid phase requires a free energy of formation $\Delta G$, given by

$$\Delta G = -N\,|\Delta\mu_{\rm N}| + \gamma\mathscr{A}, \tag{1}$$

where $\Delta\mu_{\rm N}$ is the driving force for nucleation. In the case of a pure substance, it is just the difference in chemical potentials of the solid and fluid phases under the considered thermodynamic conditions. In the case of hydrate formation, it is simply the difference between the chemical potential of the solid phase and that of the hydrate molecules in the liquid phase. $\gamma$ is the solid–liquid interfacial free energy, and $\mathscr{A}$ is the interfacial area. Since the first term is negative and grows with $N$ and the second is positive and grows with the area (i.e., $N^{2/3}$), a maximum is reached for a certain value of $N$ (i.e., the size of the critical cluster $N_c$) leading to a free energy barrier of $\Delta G_c$,

$$\Delta G_c = \frac{1}{2} N_c\,|\Delta\mu_{\rm N}|\,. \tag{2}$$

The size of the critical cluster can be obtained as

$$N_c = \frac{32\,\pi\,\gamma^3}{3\,\rho_s^2\,|\Delta\mu_{\rm N}|^3}, \tag{3}$$

where $\rho_s$ is the number density of the bulk solid phase at the considered $P$ and $T$ of the system (in CNT, one neglects changes in the density of the solid in the critical cluster due to the Laplace pressure, which is equivalent assuming that the solid phase is incompressible). The free energy barrier can also be rewritten as

$$\Delta G_c = \frac{16\,\pi\,\gamma^3}{3\,\rho_s^2\,|\Delta\mu_{\rm N}|^2}. \tag{4}$$

According to CNT, if a steady state is considered, i.e., the distribution of clusters of different sizes does not depend on time, the nucleation rate per unit volume $J$ at a given temperature $T$ is the product of the probability of a critical nucleus formation, which depends on the free energy of formation $\Delta G_c$ as $\mathscr{P}(N_c) \approx e^{-\Delta G_c/k_BT}$ and a kinetic factor $J_0$,

$$J = J_0\,e^{-\Delta G_c/k_BT} = \rho_f\,Z\,f^+\,e^{-\Delta G_c/k_BT}, \tag{5}$$

where $k_B$ is the Boltzmann constant and the $J_0 = \rho_f Z f^+$ term contains the kinetic growth information through the fluid number density $\rho_f$. $Z$ is the Zeldovich factor, which is given by

$$Z = \sqrt{\frac{|\Delta G_c''|}{2\pi k_BT}} = \sqrt{\frac{|\Delta\mu_{\rm N}|}{6\,\pi\,k_BTN_c}}. \tag{6}$$

Here, $\Delta G_c''$ is the curvature of the free energy formation at the critical size.

The attachment rate $f^+$, which can be calculated via an effective diffusion constant that accounts for the number of particles aggregated and separated in time from the critical cluster, is as follows:

$$f^+ = \frac{\langle \Delta N_c^2(t)\rangle}{2t} = \frac{\langle [N_c(t) - N_c(t_0)]^2\rangle}{2t}. \tag{7}$$

We have shown in a previous work[27] that the corresponding expression of CNT for the hydrate nucleation can be written as

$$J = \rho_L^{CO_2}\,Z\,f^+_{CO_2}\,\exp\left(\frac{-N_c^{CO_2}\,|\Delta\mu_{\rm N}|}{2\,k_B\,T}\right), \tag{8}$$

where $\rho_L^{CO_2}$ is the number density of $CO_2$ in the liquid phase, $N_c^{CO_2}$ is the number of molecules of $CO_2$ in the critical cluster (notice that the critical cluster contains both molecules of water and molecules

of $CO_2$) and $f^{+}_{CO_2}$ is the attachment rate computed from Eq. (7) by analyzing the diffusive behavior or the number of $CO_2$ molecules in the solid cluster when starting from configurations at the critical size. The value of $\gamma$ can be obtained from Eq. (3) by using $\rho_S^{CO_2}$, which is just the number density of molecules of $CO_2$ in the hydrate.

In the Seeding technique, a solid cluster is inserted into the metastable fluid at the thermodynamic conditions at which it is critical (i.e., 50% of probability of either melting or growing is determined). Once the size of the critical cluster $N_c$ (where $N_c$ is the number of $CO_2$ molecules in the solid critical cluster) is known, one determines the free energy barrier using Eq. (2). The value of $\rho_L^{CO_2}$ is determined from the solubility of $CO_2$ at the considered value of $P$ and $T$ (or with a higher value in the case of supersaturated solutions, as it will be shown later on). The only remaining ingredient is $\Delta\mu_N$, which will be described in detail in Subsection II B.

### B. Driving force for nucleation

$\Delta\mu_N$ can be viewed, as first suggested by Kashchiev and Firoozabadi[71] (also see our previous studies[27,67,72]), as a chemical reaction that takes place at constant $P$ and $T$. In fact, $\Delta\mu_N$ is just the chemical potential change of the following physical process:

$$CO_2(\mathrm{aq}, x_{CO_2}) + 5.75\ H_2O(\mathrm{aq}, x_{CO_2}) \rightarrow [CO_2(H_2O)_{5.75}]_H. \quad (9)$$

In Eq. (9), one molecule of $CO_2$ in the aqueous solution reacts with 5.75 molecules of water (also in the aqueous solution phase) to form a $[CO_2(H_2O)_{5.75}]_H$ "hydrate molecule" in the solid phase. Since we are assuming, as in our previous studies,[27,67,72] that all cages of the hydrates are filled, a unit cell of $CO_2$ hydrate is formed by 46 water molecules and 8 $CO_2$ molecules, i.e., one molecule of $CO_2$ reacts with 46/8 = 5.75 water molecules. This is consistent with the stoichiometric reaction given by Eq. (9).

Since all cages of the hydrate are occupied, the chemical potential of this compound (hydrate) can be obtained as the sum of the chemical potential of $CO_2$ in the solid plus 5.75 times the chemical potential of water in the solid [see Eq. (8) of our previous paper[72]]. Note that the chemical potentials depend on $T$ and $P$ (and on composition). However, all the results of this work were obtained for a pressure of 400 bar. For this reason, we shall omit the pressure dependence and will write the chemical potential of the hydrate simply as $\mu_H^H(T)$ (there is no dependence on composition for the hydrate as its stoichiometry is fixed). Following the work of Kashchiev and Firoozabadi[71] and our previous studies,[27,67,72] the driving force for nucleation of the hydrate formed from the aqueous solution with a concentration $x_{CO_2}$ at $T$ can be expressed as

$$\Delta\mu_N(T, x_{CO_2}) = \mu_H^H(T) - \mu_{CO_2}^{aq}(T, x_{CO_2}) - 5.75\ \mu_{H_2O}^{aq}(T, x_{CO_2}), \quad (10)$$

where $\mu_{CO_2}^{aq}(T, x_{CO_2})$ is the chemical potential of $CO_2$ in the aqueous solution, and $\mu_{H_2O}^{aq}(T, x_{CO_2})$ is the chemical potential of water in the aqueous solution.

The nucleation rate of the $CO_2$ hydrate has been determined by using BF simulations for most of the cases. In BF runs, $J$ is determined directly and it is not necessary to know the value of $\Delta\mu_N$. However, for two thermodynamic states, it was necessary to use the Seeding method, and therefore, it was necessary to obtain the value of $\Delta\mu_N$ to determine the nucleation rate. In this context, it is useful to introduce the supersaturation at a given pressure $P$ and temperature $T$ defined as

$$S = \frac{x_{CO_2}}{x_{CO_2}^{eq}}, \quad (11)$$

where $x_{CO_2}$ is the $CO_2$ molar fraction of a solution and $x_{CO_2}^{eq}$ is the $CO_2$ molar fraction under experimental conditions, i.e., the $CO_2$ concentration in water when in equilibrium with pure $CO_2$ via a planar interface at the same $P$ and $T$. In particular, we used the Seeding method for $T$ = 255 K when $S$ = 1 and when $S$ = 1.207. Note that $S$ = 1 is the setup used in the experimental work. We shall also determine $J$ from Seeding at 255 K for the case $S$ = 1.207. This case is interesting as for this particular state, it is possible to determine $J$ both from BF runs and from the Seeding method, and this state serves as a cross-check of the Seeding method (in particular, of the choice of the order parameter). The states for which we determined $J$ in this work are shown in Fig. 1, represented by diamonds and triangles.

Since Seeding is used here only for two thermodynamic states at 255 K and 400 bar, namely, $S$ = 1 and $S$ = 1.207, only the values of $\Delta\mu_N$ for these two states are needed. In our previous work,[72] the driving force for nucleation of the hydrate of $CO_2$ has been obtained using four independent methods along the solubility curve obtained when a $CO_2$-rich phase is in contact with an aqueous phase at 400 bar and several temperatures below the dissociation temperature. Particularly, we have proposed a novel methodology to evaluate the driving force for nucleation based on the calculation of partial enthalpies of $CO_2$ and water in the aqueous phase at different values of $CO_2$ composition and temperatures (we recommend reading Sec. E.4 of our previous work[72] for further details). This is a

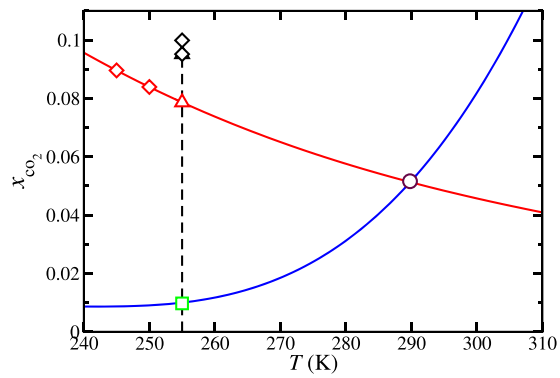


**FIG. 1.** $CO_2$ molar fraction, $x_{CO_2}$, in an aqueous solution coexisting with the hydrate (blue curve) and with a $CO_2$ fluid reservoir (red curve), as functions of temperature, at 400 bar. The diamonds and triangles represent the six states at which the nucleation rate of $CO_2$ hydrate, $J$, is obtained in this work using BF simulations (diamonds) and the Seeding technique (triangles). The red color symbols are used to denote saturated conditions ($S$ = 1), and the black color symbols denote the supersaturated conditions ($S$ > 1). Note that at 255 K and $S$ = 1.207 ($x_{CO_2}$ = 0.0969), we have estimated $J$ from BF (black diamond) and Seeding simulations (black triangle). The crossing point between both curves (maroon circle) corresponds to the temperature $T_3$ at which hydrate, solution, and $CO_2$ coexist.[67,87] The green square represents the hydrate–solution coexistence point at 255 K.

rigorous methodology obtained only from thermodynamic arguments for calculating the driving force for the nucleation of the $CO_2$ hydrate at any $P$, $T$, and $x_{CO_2}$. According to this, it is possible to directly determine the value of the driving force for nucleation at 255 K and 400 bar at the equilibrium solubility composition (i.e., $S = 1$ or $x_{CO_2} = x^{eq}_{CO_2} = 0.0803$) when a $CO_2$-rich phase is in contact with an aqueous phase via a planar interface, with it being −2.26 (in $k_BT$ units) at $S = 1$ and −2.73 (in $k_BT$ units) for $S = 1.207$. See the work of Algaba *et al.*[72] for further details and more specifically route 4 for calculating the driving force [Eq. (26) in that paper] and Fig. 14 (also there) from which these values are extrapolated.

### C. Simulation details

All molecular dynamics (MD) simulations are performed using the GROMACS package.[73,74] We use the Verlet leapfrog algorithm[75] with a time step of 2 fs. The temperature is kept constant using the Nosé–Hoover thermostat with a relaxation time of 2 ps.[76,77] The pressure is also kept constant by using the Parrinello–Rahman barostat[78] with the same relaxation time. We use two different versions of the *NPT* or isothermal–isobaric ensemble. For BF simulations and Seeding simulations under supersaturated conditions, we use the isotropic *NPT* ensemble, i.e., the three sides of the simulation box are changed proportionally to keep the pressure constant. For Seeding simulations under experimental conditions, i.e., under coexistence conditions at which the aqueous solution of $CO_2$ and the $CO_2$-rich liquid phase coexist, we use the anisotropic $NP_z\mathscr{A}T$ ensemble since a planar liquid–liquid interface exists and only fluctuations of the volume are performed by varying the length of the simulation box along the $z$-axis direction, perpendicular to the planar interface. We use a cutoff distance of 1 nm for dispersive and Coulombic interactions. For electrostatic interactions, we use the particle mesh Ewald (PME) method.[79] We do not use long-range corrections for dispersive interactions. Water and $CO_2$ molecules are described using the TIP4P/Ice[80] and TraPPE[81] models, respectively. TIP4P/Ice correctly predicts the melting point of ice Ih and that guarantees good predictions for the phase equilibria of hydrates.[82] The water–$CO_2$ unlike dispersive interactions are taken into account via the modified Berthelot rule proposed by Míguez *et al.*[83] and also used in our previous work.[72] This strategy allows us to accurately predict the three-phase $CO_2$ hydrate–water–$CO_2$ coexistence or dissociation line of the $CO_2$ hydrate. Particularly, with this choice, the dissociation temperature or $T_3$, at 400 bar, is in excellent agreement with the experimental data taken from the literature (see Fig. 10 and Table II of the work of Míguez *et al.*[83] for further details). It is also important to mention that the same molecular parameters can accurately predict the $CO_2$ hydrate–water interfacial free energy.[84–86]

The dissociation temperature or $T_3$ of the $CO_2$ hydrate at 400 bar is 290 K[72] (close to the experimental value at this pressure, which is 286 K). In this work, all simulations are carried out at 245, 250, and 255 K (supercoolings of 45, 40, and 35 K, respectively). Following our previous work,[27] we perform three different kinds of simulations to determine the nucleation rate of the $CO_2$ hydrate at 255 K: (1) BF simulations under supersaturation conditions; (2) Seeding simulations under supersaturation conditions; and (3) Seeding simulations under experimental saturated conditions. In the first set of simulations, we estimate the nucleation rate of the hydrate under two different saturated conditions using its definition and the mean first-passage time approach (MFPT). In the second set, we also determine the nucleation rate under one of the supersaturation conditions following the Seeding approach. This allows us to check if the local bond order parameters used to characterize the size of the critical cluster of the hydrate are appropriate. Finally, in the third set of simulations and once we have got the best selection of the order parameters, we estimate the nucleation rate of the $CO_2$ hydrate under experimental conditions, i.e., under the equilibrium (saturated) conditions of $CO_2$ in water in contact with a $CO_2$-rich liquid phase via a planar interface using the Seeding technique.

We perform BF simulations in the isotropic *NPT* ensemble at 255 K, placing 4942 water molecules and 530 and 560 $CO_2$ molecules, respectively (i.e., $x_{CO_2} = 0.0969$ and $x_{CO_2} = 0.1018$) in a cubic simulation box, as shown in Fig. 2(a). As the concentration of $CO_2$ in water under coexistence conditions is $x^{eq}_{CO_2} = 0.0803$,[72] the systems considered correspond to $S = 1.207$ and $S = 1.268$, respectively. In all cases, the system is equilibrated during 5–10 ns and run during up to 3 $\mu$s. This simulation time allows us to observe the formation of solid clusters of the $CO_2$ hydrate. We show in Fig. 1 some of the states for which we determined the nucleation rate at 255 K. The states simulated using BF simulations at this temperature are represented by the black triangles. In our previous studies, we have determined the dissociation temperature $T_3$ of the $CO_2$ and $CH_4$ hydrates using the so-called solubility method and calculating the crossing point (maroon circle) between the solubility curves of $CO_2$ in the aqueous solution when it is in contact with the $CO_2$ liquid phase and the hydrate, as shown in Fig. 1. This methodology has also been used in a previous work by Tanaka and co-workers (see Fig. 9 of their work).[87]

We also perform Seeding simulations at one of the two supersaturated concentrations, $S = 1.207$. According to the Seeding technique, a spherical cluster of the $CO_2$ hydrate is inserted into a supersaturated aqueous phase of $CO_2$ in water, as shown in Fig. 2(b). To do this, we first consider two bulk phases, one of $CO_2$ hydrate and another of an aqueous solution of $CO_2$ with the appropriate supersaturation ($S = 1.207$), at 255 K and 400 bar. The aqueous solution of $CO_2$ is identical to that used in the BF simulations (4942 water molecules and 530 $CO_2$ molecules). The hydrate simulation box is formed from 2944 molecules of water and 512 $CO_2$ molecules. This corresponds to a $4 \times 4 \times 4$ unit cell of sI hydrate structure with full occupancy. The space group of the unit cell is $Pm\bar{3}n$. The proton disorder was obtained using the algorithm of Buch *et al.*[88] Both simulation boxes are equilibrated in the *NPT* ensemble separately. The hydrate system is equilibrated during 50 ns. After this time, a spherical cluster of radius ranging from 1 to 1.4 nm is cut and immersed into the saturated aqueous solution of $CO_2$ in water. This is practically done by removing water and $CO_2$ molecules and creating a spherical empty space with the same radius of seed of the spherical hydrate cluster. Overlaps in the interface are avoided by slightly moving or rotating nearby molecules. We recommend our previous work to the reader for further details.[67]

In addition, we run Seeding simulations under coexistence conditions, i.e., the hydrate cluster is inserted into a solution in equilibrium with a $CO_2$-rich liquid phase via a planar interface at 255 K and 400 bar. This corresponds to a molar fraction of $CO_2$

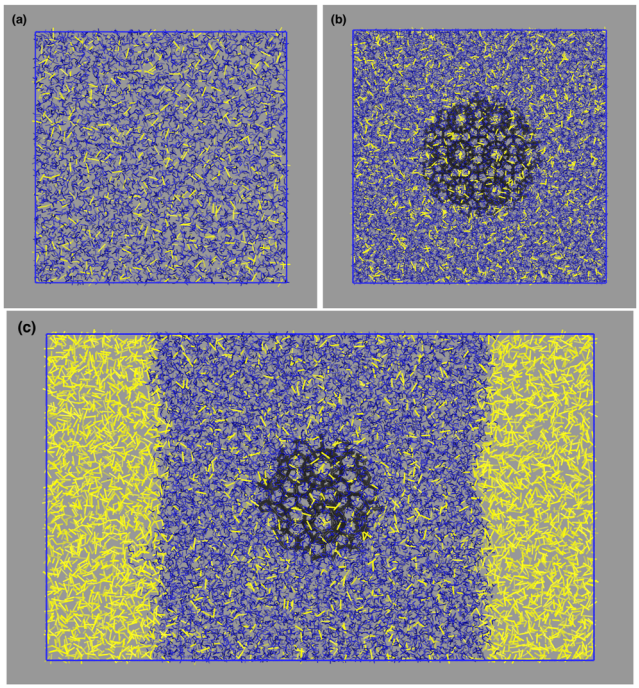


**FIG. 2.** Starting configurations for runs performed in this work to estimate nucleation rates at 400 bar and different temperatures and concentrations. Water and $CO_2$ molecules are represented by the blue and yellow sticks, respectively. The black molecules depict the spherical seed of the $CO_2$ hydrate introduced into the system to induce crystallization. (a) One-phase system of a supersaturated aqueous solution of $CO_2$ ($5.57 \times 5.57 \times 5.57$ nm$^3$). (b) Two-phase system with a solid cluster of the $CO_2$ hydrate (seed) inserted in the aqueous solution of $CO_2$ at saturation $S > 1$ ($5.58 \times 5.58 \times 5.58$ nm$^3$). (c) Three-phase system with a $CO_2$ liquid phase in contact with an aqueous solution of $CO_2$ via a planar interface and a spherical cluster of $CO_2$ hydrate inserted in the aqueous solution of $CO_2$ ($7.40 \times 7.40 \times 12.41$ nm$^3$). In this case, the concentration of $CO_2$ in water is that of equilibrium ($S = 1$). The size of the simulation boxes is given in terms of average values since it fluctuates in *NPT* simulations. In case of panel (c), simulations are performed in the $NPz\mathscr{A}T$ ensemble so that $L_x$ and $L_y$ are fixed and $L_z$ fluctuates around the average value.

in water $x_{CO_2} = x^{eq}_{CO_2} = 0.0803$. This state corresponds to the red triangle represented in Fig. 1 at 255 K.

To keep this concentration constant, the hydrate seed is inserted into the aqueous solution in contact with a $CO_2$-rich liquid phase, as shown in Fig. 2(c). In this case, since there is a planar interface in the simulation box, we perform the simulations in the $NP_z\mathscr{A}T$ anisotropic ensemble. The aqueous solution–$CO_2$ system is formed from 12 000 water molecules and 4952 $CO_2$ molecules; these are the total number of molecules of the whole system, the aqueous solution of $CO_2$ and the $CO_2$ liquid reservoir. Once the system is properly equilibrated, the spherical hydrate is inserted at the center of the aqueous phase in the same way as in the Seeding simulations under supersaturated conditions.

Finally, we also perform additional BF simulations at 245 and 250 K (at 400 bar in both cases). In both cases, however, simulations are performed at $S = 1.0$. i.e., at the corresponding $CO_2$ saturation concentration. These two states correspond to the red diamonds represented in Fig. 1 at 245 and 250 K. We use two types of simulation setups for this study: a homogeneous $CO_2$-saturated bulk solution and a saturated solution in contact via a planar interface with a fluid $CO_2$ reservoir. In the first case, we use isotropic *NPT* runs. In the second one, we use $NP_z\mathscr{A}T$ runs. The reason to determine $J$ in these two different setups is that we want to investigate if the presence of an interface between $CO_2$ and water enhances/hinders or has no effect on the nucleation rate. At 245 K, we use 2400 and 240 water and $CO_2$ molecules in the homogeneous system (cubic simulation box with a volume of 82.5 nm$^3$), respectively, and 2400 and 1148 water and $CO_2$ molecules, respectively, in the inhomogeneous system (volume of the simulation box equal to 4141.9 nm$^3$). This corresponds in both cases to a molar fraction of $CO_2$ in water $x_{CO_2} = x^{eq}_{CO_2} = 0.09$. At 250 K, we use 6524 and 606 water and $CO_2$ molecules, respectively, in the homogeneous system and 7200 and 3444 water and $CO_2$ molecules, respectively, in the inhomogeneous system. As in the previous case, in the homogenous system, we use a cubic simulation box with a volume of 222.5 nm$^3$. In the inhomogeneous system, the volume of the simulation box is 420.1 nm$^3$. In this case, the molar fraction of $CO_2$ in water $x_{CO_2} = x^{eq}_{CO_2} = 0.085$.

It is important to recall here that the size of our system, as well as the number of molecules forming the systems in which BF and Seeding simulations are performed at 255 K (at different supersaturations), have been appropriately selected. Note that we have used the same size for the simulation box and number of water molecules as in our previous work for $CH_4$ hydrates.[67] The number of $CO_2$ molecules is different since the molar fraction in the aqueous solution is different. In BF simulations, when the hydrate cluster size is greater than a threshold ($n_h = 125$ in this work as is shown in Sec. III B), the number of $CO_2$ molecules in the cluster is $125/5.75 \approx 22$, assuming full occupancy of the hydrate, i.e., $46/8 = 5.75$ water molecules per $CO_2$ molecule. This means that the molar fraction in the aqueous solution surrounding the hydrate cluster is 0.0954 and 0.1007 for $S = 1.207$ and 1.268, respectively. Comparing these values with those at the beginning of the simulations, 0.0969 and 0.1018, the variation in $x_{CO_2}$ when a hydrate cluster grows irreversibly is less than 1.6%. Consequently, we think the concentration of $CO_2$ in aqueous solution does not substantially decrease as the hydrate size grows.

In addition, Weijs *et al.*[89] have reported the existence of a diffusive shielding effect in simulations involving nanobubble clusters that help stabilize them. We believe that there is no diffusive shielding effect in our simulations. The simulation boxes and system sizes used in this work are similar to those employed in our previous work on $CH_4$ hydrates,[67] where we did not detect such an effect. For instance, in BF simulations with $S = 1.207$ performed in this work, the radius of the largest cluster formed from more than 125 water molecules (threshold value mentioned in the previous paragraph) is lower than $r = 1.04$ nm. According to this, the minimum distance between any two molecules from the cluster and its periodic image is higher than 3.5 nm, which corresponds to $3.5 \times r_c$ with $r_c$ being the cutoff distance. This confirms that there are no interactions between a cluster and its periodic images. Furthermore, it is worth noting that, within statistical error, one single hydrate cluster is detected in our simulations using the $\overline{q}_3 - \overline{q}_{12}$ combination of order parameters.

## III. RESULTS

### A. Order parameter

In general, the size of the largest solid cluster is an adequate order parameter in nucleation studies. To identify the size of the largest solid cluster, it is necessary to identify solid and fluid molecules first. A good order parameter should label most of the molecules as fluid when they are in the bulk fluid phase or as solid when they are in the bulk solid phase. The mislabeling (i.e., molecules labeled as solid in the bulk fluid and as liquid in the bulk solid) should be as small as possible and equal in both phases.[23] To identify water solid particles, we use the averaged order parameters proposed by Lechner and Dellago.[90] In previous studies, we have shown that $\bar{q}_{12}$ does a very good job in identifying water molecules in the solid $CH_4$ hydrate[27] but also in other hydrates.[91] Here, we shall use a combination of $\bar{q}_3$ and $\bar{q}_{12}$ since it provides even better results. Oxygen atoms (and not hydrogen ones) were used when computing the order parameter. To obtain either $\bar{q}_3$ or $\bar{q}_{12}$ of each water molecule, we considered all the water molecules at a distance of 5.5 Å or less from the molecule of interest (this distance corresponds to the second minimum of the radial distribution function).

We carried out simulations in bulk phases: $CO_2$ hydrate and aqueous solution of $CO_2$ at 255 K and 400 bar. The $\bar{q}_3$ and $\bar{q}_{12}$ values obtained after 50 ns of production are plotted in Fig. 3. As can be seen, this pair of parameters allows clearly differentiating between the cloud of water molecules in the hydrate phase and that of water in the dissolution. From the values plotted in Fig. 3, we determine a threshold function that is a linear combination of $\bar{q}_3$ and $\bar{q}_{12}$ parameters being $\bar{q}_c = -0.6718\,\bar{q}_3 + 0.1484$, with the best separation causing a mislabeling of just 0.018%. Thus, this order parameter is exceptionally good at identifying solid and fluid particles. Finally, to determine the number of water molecules in a solid cluster, we consider two molecules connected if they are labeled as solid and their separation is less than 3.5 Å. The number of $CO_2$ is inferred by the hydrate stoichiometry 1 $CO_2$: 5.75 $H_2O$.

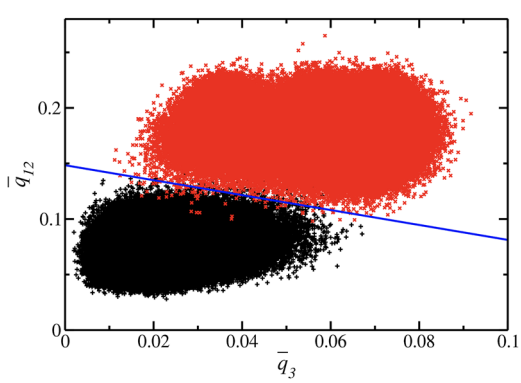


**FIG. 3.** Averaged local bond order parameters $\bar{q}_3$ and $\bar{q}_{12}$ of water molecules for bulk systems at 255 K and 400 bar. The black pluses correspond to water molecules in the aqueous solution of the $CO_2$ phase at equilibrium concentration $x^{eq}_{CO_2}$; the red crosses represent water molecules in the hydrate phase; and the threshold with minimum mislabeling[23] between the two phases is indicated by the blue line $\bar{q}_c = -0.6718\,\bar{q}_3 + 0.1484$.

It is simple to locate the transition to the solid phase using BF simulations if one has an order parameter that distinguishes reasonably well fluid and solid particles. Estimated nucleation rates do not depend on the choice of the order parameter. However, in the case of Seeding, things are different. The estimate of $J$ will depend on the choice of the order parameter. Ideally, one should use an order parameter that allows correctly estimating the radius at the surface of tension of the solid cluster (see previous work for a deeper discussion of this point). In our previous work,[27] we have demonstrated that the $\bar{q}_{12}$ local bond order parameters of Lechner and Dellago[90] is a good choice to get accurate estimates for the nucleation rates of the methane hydrate. Some of us have recently shown that the same is true when the $\bar{q}_3 - \bar{q}_{12}$ combination is used for the methane hydrate, as well as for other hydrates, including nitrogen, hydrogen, and tetrahydrofuran hydrates.[91] It is necessary to show now that the $\bar{q}_3 - \bar{q}_{12}$ combination is also providing good estimates of $J$ for the $CO_2$ hydrate within the Seeding formalism. The way to test that is to compare values obtained of $J$ from BF simulations to those obtained from Seeding.

### B. Nucleation rate by BF simulations at 255 K and supersaturations $S$ = 1.207 and $S$ = 1.268

At 255 K and 400 bar, when $S = 1$ we were unable to nucleate hydrates in the two phases system ($CO_2$ and water) within our computational resources (several thousand molecules and up to 10 $\mu$s simulations). For this reason, we decided to consider two supersaturated solutions at 255 K and 400 bar, one with $S = 1.207$, which corresponds to a molar fraction of $x_{CO_2} = 0.0969$, and another with $S = 1.268$, which corresponds to $x_{CO_2} = 0.1016$. Note that although both molar fractions are close to the equilibrium concentration of $CO_2$ in water under coexistence conditions, $x^{eq}_{CO_2} = 0.0803$,[72] the time required to observe nucleation in BF simulations is very different (see in the following). The typical volume of the simulation box was 172.4 nm$^3$ ($S = 1.207$) and 173.4 nm$^3$ ($S = 1.268$) (containing 4942 molecules of water and 530 or 560 molecules of $CO_2$, respectively). Runs were done in the isotropic *NPT* ensemble.

Figure 4 shows the number of water molecules in the largest solid cluster of the $CO_2$ hydrate, $n_h$, as a function of time for systems with supersaturations $S = 1.207$ and 1.268. In the first case ($S = 1.207$), shown in panel (a), we have considered 15 independent trajectories, and in the second case ($S = 1.268$) shown in panel (b), we have simulated 20 trajectories. For each run, we determine the nucleation time as the one required to cross the horizontal line defined by $n_h > 125$ as this corresponds to a post-critical cluster that never returns to the fluid phase and grows irreversibly. For $S = 1.268$, the twenty trajectories are successful in nucleating the solid phase in less than 1 $\mu$s. For $S = 1.207$, 12 of 15 were successful after runs of up to 3 $\mu$s. Let us now compute the nucleation rate. For the case $S = 1.268$, the nucleation rate can be estimated simply as

$$J_{BF} = \frac{1}{\tau V}, \tag{12}$$

where $\tau$ is the average time required for the system to nucleate. For $S = 1.268$, it is easy to determine this time obtaining a value of about $2 \times 10^{31}/(\text{m}^3\ \text{s})$. For $S = 1.207$, not all trajectories are successful in nucleating the solid. In this case, $\tau$ could be computed from the time

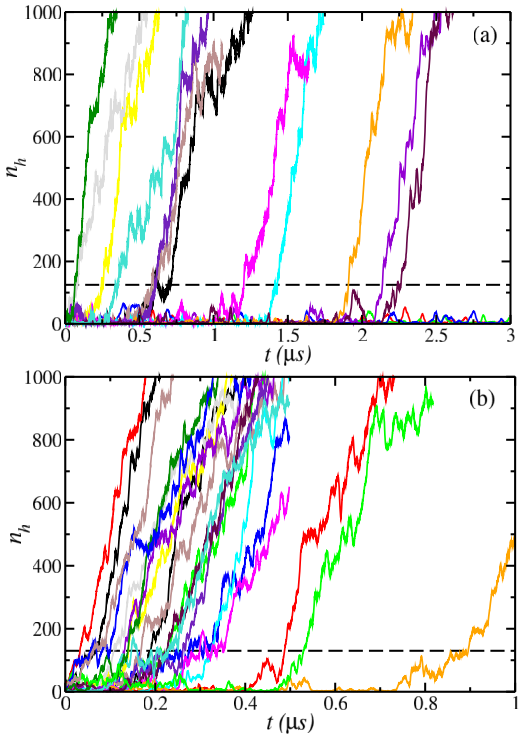


**FIG. 4.** Number of water molecules in the largest cluster of the $CO_2$ hydrate, $n_h$, as a function of time, with supersaturation $S = 1.207$ (a) and 1.268 (b). The cluster size is obtained using the $\bar{q}_3 - \bar{q}_{12}$ linear combination of order parameters. Each curve represents an independent BF *NPT* simulation at 255 K, 400 bar, and the corresponding saturation. The dashed horizontal line in each panel represents a post-critical cluster that always grows irreversibly and that can be used to determine the nucleation time of each individual run.

required to nucleate $n$ trajectories out of $n_0$ by using the following expression:

$$\tau = \frac{\tau_{(n_0-n)/n_0}}{\ln\left(\frac{n_0}{n_0-n}\right)}. \tag{13}$$

Since we have performed 15 different trajectories, $n = 12$ and $n_0 = 15$, and consequently $\tau_{3/15} = 2240$ ns. Using this result, the volume of the simulation box, $V = 172.4$ nm$^3$, and combining Eqs. (12) and (13), the nucleation rate of the $CO_2$ hydrate in the supersaturated solution with $S = 1.207$ is $J_{BF} = 4.2 \times 10^{30}/(\text{m}^3\ \text{s})$.

Alternatively, one could follow the work of Walsh *et al.*[49] and estimate $\tau$ as the total simulated time (including the full length of the run for non-successful trajectories and the time for nucleation in the successful ones and dividing by the number of successful runs, which is 12 in this case). The final value using this route is $J_{BF} = 3.4 \times 10^{30}/(\text{m}^3\ \text{s})$, which is in excellent agreement with the value obtained using the $\tau_{3/15}$ value.

A different route to determine $J$ is performing a MFPT analysis. In MFPT analysis, $\tau(N)$ is the average elapsed time until the largest cluster of the system reaches or exceeds a threshold size $N$ for the first time. Under reasonably high barriers, $\tau(N)$ is given by the following expression:[92,93]

$$\tau(N) = \frac{\tau_J}{2}\left\{1 + \text{erf}\left[Z\sqrt{\pi}(N - N_c)\right]\right\}, \tag{14}$$

where $\text{erf}(x)$ is the error function, $Z$ is the Zeldovich factor, $N_c$ is the critical nucleus size, and $\tau_J = 1/J$ is the inverse of the steady-state nucleation rate $J$. This expression works well when the growth's time scale is small compared to the time scale for nucleation. Alternatively, when they are comparable, one could fit the results into the following expression:

$$\tau_{\text{mod}}(N) = \tau(N) + \frac{1}{2G}(N - N_c)\{1 + \text{erf}[C(N - N_c)]\}, \tag{15}$$

where $G$ is the growth rate and $C$ is a positive constant and $\tau(N)$ is given by Eq. (14). In Fig. 5, a MFPT analysis is performed and the results are fitted to both Eqs. (14) (red lines) and (15) (blue lines). The value of $J$ is obtained from the MFPT analysis as

$$J_{\text{MFPT}} = \frac{1}{\tau_J V}. \tag{16}$$

The results for the nucleation rate obtained from the MFPT analysis are shown in Table I. Note that the results of Fig. 5 show

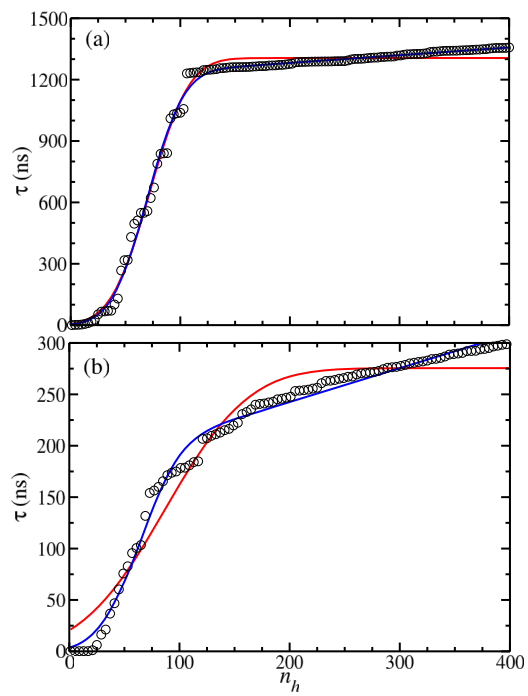


**FIG. 5.** MFPT, τ, as a function of the largest cluster size, $n_h$, obtained for the solution of CO2 in water at 255 K and 400 bar with supersaturation S = 1.207 (a) and 1.268 (b). Note that $n_h$ is given in terms of the number of water molecules in the hydrate phase. The black circles correspond to the average time at which the cluster of water molecules in the hydrate phase reaches for the first time a certain size in the range from 0 to 400 molecules according to the BF simulations plotted in Fig. 4. Continuous curves are fitted using Eqs. (14) (red curve) and (15) (blue curve).

**TABLE I.** Nucleation rate of $CO_2$ hydrate in water, $J$, at 255 K, 400 bar, and supersaturation S = 1.207 and S = 1.268 using the MFPT method.

| $S$ | 1.207 | | 1.268 | |
|---|---|---|---|---|
| | Equation (14) | Equation (15) | Equation (14) | Equation (15) |
| $\tau_j$ (ns) | 1305.6 | 1232.4 | 275.5 | 197 |
| $Z$ | 0.014 | 0.015 | 0.007 | 0.013 |
| $N_c^{H_2O}$ | 72.2 | 69.8 | 86.7 | 61.7 |
| $G$ ($ns^{-1}$) | ⋯ | 2.64 | ⋯ | 3.03 |
| $C$ | ⋯ | 0.19 | ⋯ | 179.7 |
| $V$ ($nm^3$) | 172.4 | 172.4 | 173.4 | 173.4 |
| $J$ ($m^{-3}$ $s^{-1}$) | $4.4 \times 10^{30}$ | $4.7 \times 10^{30}$ | $2.1 \times 10^{31}$ | $2.9 \times 10^{31}$ |

that for the two supersaturations studied ($S$ = 1.207 and 1.268), the solid is formed by the nucleation of just one critical cluster (after an induction time), followed by growth. However, for much higher supersaturations, one would expect the appearance of multiple small critical clusters so that the solid could grow via the growth of these individual clusters[93] and by the Ostwald ripening mechanism.[89,94]

The summary is that BF simulations lead to values of $J$ of about $4 \times 10^{30}$ and $2 \times 10^{31}/(m^3\ s)$ for $S$ = 1.207 and $S$ = 1.268, respectively. For methane hydrate, one obtained similar values of $J$ for $S$ = 4.72 and 5.67, respectively. Thus, nucleation of $CO_2$ hydrate is easier since it appears at lower supersaturations. What provokes this enhancement of homogeneous nucleation in the $CO_2$ hydrate? Certainly $CO_2$ is about one order of magnitude more soluble than $CH_4$ at the same pressure and supercooling (i.e., $x_{CO_2}$ = 0.0803 for $CO_2$ vs $x_{CH_4}$ = 0.0089 for methane). However, $CH_4$ seems more efficient. In fact, it is able to reach values of $J$ of the order of $10^{30}$ with a concentration of $x_{CH_4}$ = 0.042, whereas for $CO_2$, one needs a concentration of $x_{CO_2}$ = 0.097 to obtain the same nucleation rate (a similar conclusion was obtained in a previous work by some of us on the growth rate of the hydrate[95]). Later in this paper, we will try to identify the key ingredient that makes the homogeneous nucleation of the $CO_2$ hydrate much easier.

The values of $J$ for $S$ = 1.207 of this section will allow determining if the choice of order parameters to distinguish between hydrate-like and liquid-like water molecules can be used with confidence to correctly determine nucleation rates when using the Seeding technique. Note that $J$ values using this technique are quite sensitive to the choice of the order parameter in contrast with BF runs, which do not depend much on the choice of the order parameter.

### C. Nucleation rate from Seeding simulations at $T$ = 255 K and supersaturation $S$ = 1.207

The Seeding method was implemented as follows: after equilibrating a one-phase system using isotropic $NPT$ simulations at 255 K and 400 bar with $S$ = 1.207, we inserted spherical hydrate seeds of different sizes as it is schematized in Fig. 2(b). After insertion, we removed particles that overlap with the solid cluster and allowed for a short run where the seed molecules were frozen. After that, several $NPT$ runs (with all molecules free to move) with different initial random velocities were performed. When the seed was small,

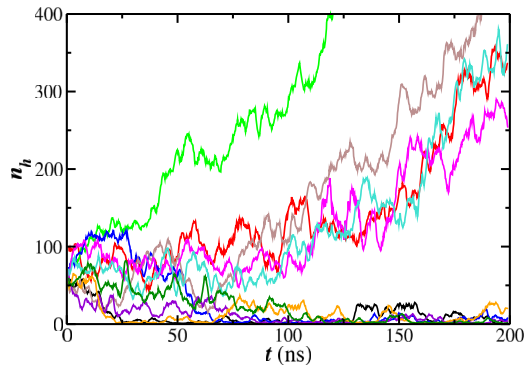


**FIG. 6.** Number of water molecules in the largest cluster of the $CO_2$ hydrate, $n_h$, as a function of time, for a supersaturated solution of $CO_2$ in water ($S$ = 1.207) at 255 K and 400 bar. The starting configuration contains a seed of hydrate of radius $r$ = 0.79 nm, which is critical under these conditions. The average size of the cluster, $N_c^{H_2O}$ = 55, is obtained using the $\bar{q}_3 - \bar{q}_{12}$ linear combination shown in Fig. 3.

the solid cluster quickly melted. When the seed was large, the solid cluster grew. Just at the critical size, there is a 50% probability that the hydrate grows or melts. We considered nine different cluster sizes: $r$ = 0.51, 0.61, 0.68, 0.74, 0.79, 0.85, 0.87, 0.91, and 0.95 nm, each of them formed from 15, 25, 35, 45, 55, 65, 75, 85, and 95 water molecules in average, respectively. For each cluster size, we have performed ten different simulations. We have observed that for spherical hydrate seeds with a radius lower than 0.74 nm, only 2 or 3 trajectories grow (2 of 10 for the two lowest radii and 3 of 10 for $r$ = 0.68 nm). On the contrary, for spherical hydrate seeds with a radius equal or greater than 0.86 nm, most of the trajectories grow (6 of 10 for $r$ = 0.85 nm and 9 of 10 for $r \geq 0.87$ nm). According to this, the spherical hydrate seed that can be considered critical is that with $r$ = 0.79 nm, formed from 55 water molecules. As can be seen in Fig. 6, when a spherical hydrate seed of radius $r$ = 0.79 nm is inserted into the supersaturated solution $S$ = 1.207, at 255 K and 400 bar, the system behaves as critical, showing five trajectories for which the inserted seed grows and 5 in which rapidly melts. The initial size of the seed is calculated by averaging the largest cluster size during the equilibration period of 2 ns in all runs using the selected parameters.

Once we know the critical cluster size, the attachment rate $f^+_{CO_2}$ can be calculated by averaging the squared difference between the initial cluster size and the cluster size in time. This term behaves linearly and $f^+_{CO_2}$ is defined as half of the slope of the linear fit according to Eq. (7). Applying this formula to all Seeding runs, we obtain the behavior plotted in Fig. 7 and $f^+_{CO_2} = 1.68 \times 10^9\ /(s)$. In addition, from our previous work, the driving force under these thermodynamic conditions is $\Delta\mu_N = -2.73 k_B T$. In this way, the Zeldovich factor, Eq. (6) is $Z$ = 0.123 and using Eq. (8), we have estimated the nucleation rate $J = 1.4 \times 10^{30}/(m^3\ s)$ for a supersaturated solution $S$ = 1.207 at 255 K and 400 bar via the Seeding approach. As can be noticed, this result is in complete agreement with the findings using BF simulations. According to this, the linear combination of $\bar{q}_3$ and $\bar{q}_{12}$ can be safely used to describe the correct cluster size. The results of this section are summarized in Table II.

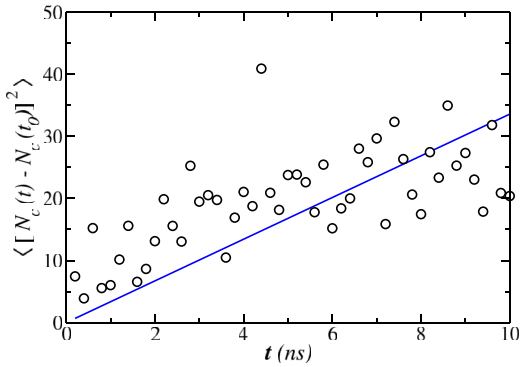


**FIG. 7.** $\langle [N_c(t) - N_c(t_0)]^2 \rangle$ factor, given in terms of $CO_2$ molecules, averaged over ten independent simulations of a supersaturated solution of $CO_2$ in water ($S = 1.207$) with the critical seed of hydrate at 255 K and 400 bar plotted in Fig. 6. The black circles represent values obtained from simulations, and the blue line represents the linear fit of the simulation results.

**TABLE II.** Nucleation rate of $CO_2$ hydrate in water, $J$, at 255 K, 400 bar, and supersaturations $S = 1$ and 1.207 using the Seeding methodology.

| $S$ | 1.0 | 1.207 |
|---|---|---|
| $N_c^{H_2O}$ | 115 | 55 |
| $N_c^{CO_2}$ | 20 | 9.6 |
| $Z$ | 0.077 | 0.123 |
| $\Delta G_c$ ($k_B T$) | 22.6 | 13.06 |
| $f^+_{CO_2}$ ($s^{-1}$) | $6.54 \times 10^8$ | $1.68 \times 10^9$ |
| $J$ ($m^{-3}\ s^{-1}$) | $2 \times 10^{25}$ | $1.36 \times 10^{30}$ |
| $\gamma$ ($mJ/m^2$) | 18.66 | 17.63 |

### D. Seeding simulations of BF clusters at $T = 255$ K and supersaturation $S = 1.207$

The formation of hydrates from solutions with appropriate composition of the guest component using BF simulations exhibits multiple pathways, including amorphous agglomeration of cages, partially ordered hydrates, and mixtures of different crystal structures among others, as clearly explained by Guo, Zhang, and collaborators.[96,97] The nuclei formed during BF simulations may not exhibit the thermodynamically stable sI crystallographic structure, although as Zhang *et al.*[97] have shown, it is possible to get a spontaneously formed cluster with a high degree of sI crystallinity. Jacobson and Molinero have also analyzed the role of amorphous intermediates in the formation of clathrate hydrates.[98]

In Sec. III B, we have obtained estimations of the $CO_2$ hydrate nucleation rate at 255 K and 400 bar, with supersaturation $S = 1.207$, from BF simulations. The value reported there is $J_{BF} \sim 10^{30}\ m^{-3}\ s^{-1}$. We have also used the Seeding technique to estimate the nucleation rate of the hydrate under the same thermodynamic conditions and supersaturation (Sec. III C). The value obtained is of the same order of magnitude, $J \sim 10^{30}\ m^{-3}\ s^{-1}$. It is possible to analyze the clusters used in BF and Seeding simulations to obtain additional information from these two embryos. Particularly, one could use a nucleus generated from BF simulations as a seed in Seeding simulations, i.e., to insert a nucleus formed during BF simulations. This allows us to check if two hydrate clusters formed from the same number of molecules, one obtained from BF simulations and a perfect (sI) and a spherical one usually used in Seeding simulations, are critical. Following this approach, we have randomly selected a trajectory of our BF simulations with $S = 1.207$ (one of those shown in Fig. 4) and picked up a solid hydrate cluster formed from 55 water molecules from the corresponding trajectory. Figure 8 shows a snapshot of this cluster that has the same number of water molecules as the critical one used in the Seeding

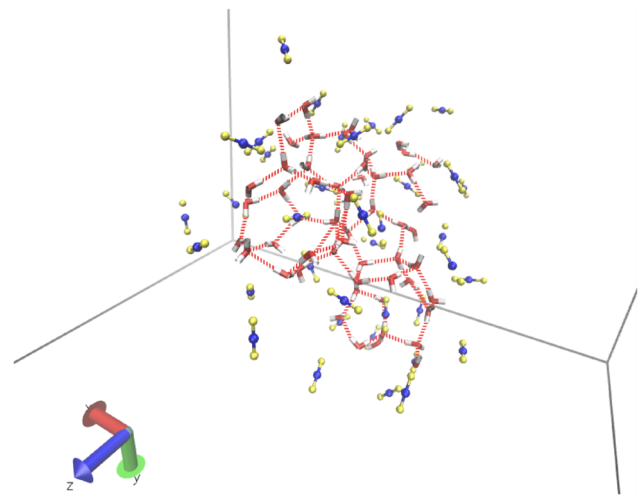

**FIG. 8.** Snapshot of cages of the $CO_2$ hydrate taken from a BF simulation, with $S = 1.207$, at 255 K and 400 bar, forming a cluster with 55 water molecules. This cluster has been extracted from one of the BF trajectories shown in Fig. 4(a). Water molecules are represented using red sticks for the oxygen atoms and white ticks for the hydrogen atoms. The red dashed lines represent hydrogen bonds between the molecules of water in the cluster, and $CO_2$ molecules are represented using blue sticks for the carbon atoms and red yellow for the oxygen atoms.

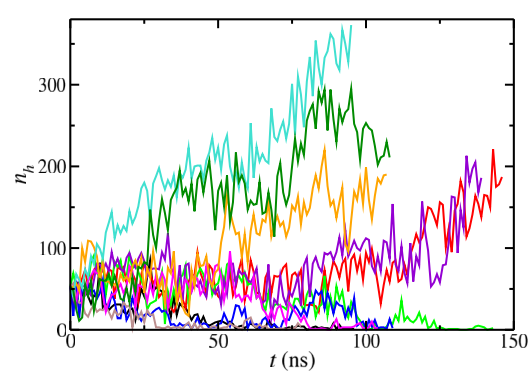


**FIG. 9.** Number of water molecules in the largest cluster of the $CO_2$ hydrate, $n_h$, as a function of time, for a supersaturated solution of $CO_2$ in water ($S = 1.207$) at 255 K and 400 bar. The starting configuration contains a seed of hydrate from BF simulations under the same thermodynamics conditions. The starting size of the cluster, $N_c^{H_2O} = 55$, is obtained using the $\bar{q}_3 - \bar{q}_{12}$ linear combination shown in Fig. 3.

simulations (see Table II). We insert the cluster obtained from BF simulations in the aqueous solution as it was done in Sec. III C and run ten different independent trajectories. If the BF cluster is critical, the system should show five trajectories for which the inserted seed grows and 5 in which it rapidly melts. Figure 9 shows the number of water molecules of this $CO_2$ hydrate cluster, $n_h$, as a function of time, in the supersaturated solution of $CO_2$ in water ($S = 1.207$) at 255 K and 400 bar. As can be seen, our results indicate that the cluster obtained from BF simulations, with the same size as a cluster that is critical according to Seeding simulations, is also critical (at the studied conditions). It should be noted that Guo and Zhang[99] found smaller sizes of the critical cluster when amorphous clusters were considered when compared to crystalline ones. This is an interesting observation that deserves to be analyzed in more detail in the future. However, at least for the case considered here ($S = 1.207$), we found that the size of a crystalline critical cluster and a critical cluster obtained from BF simulations is rather similar.

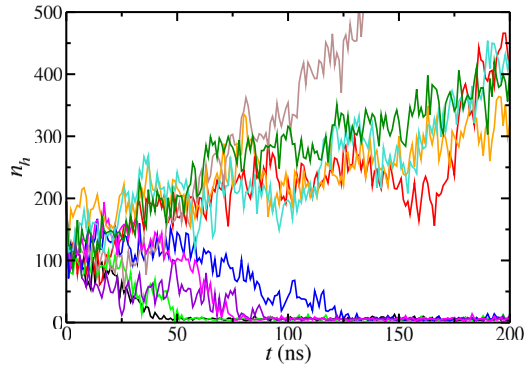


**FIG. 10.** Number of water molecules in the largest cluster of the $CO_2$ hydrate, $n_h$, as a function of time, for the saturated solution of $CO_2$ in water ($S = 1$) at 255 K and 400 bar. The starting configuration contains a seed of hydrate of radius $r = 1.01$ nm, which is critical under these conditions. The average size of the cluster, $N_c^{H_2O} = 115$, is obtained using the $\bar{q}_3 - \bar{q}_{12}$ linear combination of the local bond order parameters.

### E. Nucleation rate by Seeding simulations at $T = 255$ K and $S = 1$

We were not able to nucleate the hydrate in BF runs at 255 K and 400 bar when having the two-phase system with $CO_2$ and water at equilibrium (i.e., $S = 1$). Thus, we shall use the Seeding method to estimate the nucleation rate after having validated the technique with the results of Subsection III D. The Seeding method was implemented as follows: we first constructed the starting configuration, as shown in Fig. 2(c), by equilibrating in the isotropic $NPT$ ensemble a cubic simulation box formed from 12 000 water molecules and 1048 $CO_2$, i.e., $x_{CO_2} = 0.0803$ ($S = 1$). Once the temperature, pressure, and average volume achieved a constant value, we add a reservoir of liquid $CO_2$ at both sides of the previous dissolution, forming two planar interfaces with 4952 $CO_2$ molecules in total, including the reservoir and solution. The $z$-axis direction is perpendicular to the $CO_2$–water interface. Again, this two-phase system is equilibrated in an $NP_z\mathscr{A}T$ ensemble keeping constant the cross-section area, $\mathscr{A}$, with the value being the average area found in the equilibration part before putting the reservoir. We now inserted spherical seeds of $CO_2$ hydrate with radius ranging between 1.0 and 1.5 nm in the middle of the aqueous phase, removed overlapping particles in the solution, and equilibrated for one or 2 ns. We then performed $NP_z\mathscr{A}T$ runs. The length of these runs was about 200 ns. The size of the system (although it fluctuates in the $z$ direction) is about $7.4 \times 7.4 \times 12.4$ nm$^3$.

The size of the largest cluster, as a function of time, is plotted in Fig. 10 for an initial seed of radius $r = 1.01$ nm. As can be seen, when the size of the largest cluster is about 115(5) water molecules, the cluster becomes critical and thus the seed melts in half of the trajectories and grows in the other half. Notice that this number of water molecules in the hydrate phase corresponds to 19(1) $CO_2$ molecules also in this phase. The attachment rate can be calculated through the linear fit of $\langle [N_c^{CO_2}(t) - N_c^{CO_2}(t_0)]^2 \rangle$, as a function of time, under this condition as is shown in Fig. 11. In this case, we estimate $f^+_{CO_2} = 6.54 \times 10^8$ s$^{-1}$. Using Eq. (2), we find that the free energy barrier of nucleation for the system of $CO_2$ in water at 255 K, 400 bar, and concentration $S = 1$ is $\Delta G_c = 22(2) k_B T$, which is about five times less than that in the case of $CH_4$ in water at the same supercooling ($\Delta G_c = 95 k_B T$, as we found in our previous work[27]). The Zeldovich factor is thus $Z = 0.077$, and the nucleation rate estimated using the linear combination of the $\bar{q}_3$ and $\bar{q}_{12}$ order parameters and Eq. (8) is $J = 2(5) \times 10^{25}$ m$^{-3}$ s$^{-1}$. All the results required to estimate the nucleation rate from Seeding are shown in Table II. Our estimate of $J$ at 255 K and 400 bar, for $S = 1$ (i.e., under experimental conditions), namely, $J = 2(5) \times 10^{25}$ m$^{-3}$ s$^{-1}$ is consistent with the value reported at 260 K and 500 bar by Arjun and Bolhuis,[58] $J = 1 \times 10^{26}$ m$^{-3}$ s$^{-1}$. However, it should be noticed that (1) the force field used here is similar but not identical to that used by Arjun and Bolhuis (here, we include deviations from the Lorentz–Berthelot energetic combining rule for the interaction between the carbon atom of $CO_2$ and the oxygen of water in contrast to Arjun and Bolhuis); (2) the thermodynamic conditions are slightly different; and (3) Arjun and Bolhuis used a bubble of $CO_2$ as a reservoir and, therefore, the solubility of the gas was higher than that of the planar interface implemented in this work. In any case, even taking these differences into account, it seems that the results of this work are consistent with those of Arjun and Bolhuis.[58]

The homogeneous nucleation rate under experimental conditions for 400 bar and 35 K of supercooling is huge. In fact, it is about 30 orders of magnitude larger than that found for methane under the same conditions (it was found of the order of $10^{-7}$ m$^{-3}$ s$^{-1}$). Note that the comparison is performed at the same pressure (400 bar) and supercooling ($\Delta T = 35$ K). Therefore, homogeneous nucleation is significantly more important in $CO_2$ than in $CH_4$ and will be present in experiments at much higher temperatures. This leads to a very interesting question: what is the factor provoking such a huge difference of $J$ value? In this context, it is relevant to mention the work of Zhang *et al.*[68] These authors proposed a novel explanation for the dependence of the self-diffusion coefficient of guest molecules on guest concentration. They suggested that the higher mobility of $CO_2$ in water, compared to $CH_4$, necessitates a greater concentration of $CO_2$ in water (relative to methane) to induce nucleation. In other words, they established a connection

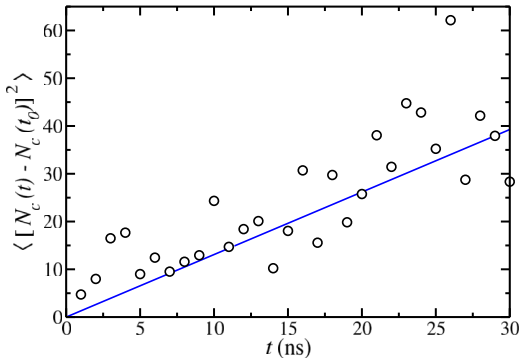


**FIG. 11.** $\langle [N_c(t) - N_c(t_0)]^2 \rangle$ factor, given in terms of $CO_2$ molecules, averaged over ten independent simulations of the saturated solution of $CO_2$ in water ($S = 1$) with the critical seed of hydrate at 255 K and 400 bar plotted in Fig. 10. The black circles represent the values obtained from simulations, and the blue line represents the linear fit of the simulation results.

between guest dynamics and hydrate nucleation. However, as we demonstrate in Sec. III E, although there could be a contribution of the $CO_2$ mobility, we believe that the primary factor behind the 30-order-of-magnitude difference in nucleation rates is the disparity in interfacial free energy between the hydrate and aqueous solution for each hydrate. Interestingly, the mobility only enters in the attachment rate, which exhibits similar values in both hydrates under the conditions considered in this work ($f^+_{CO_2} \approx 6 \times 10^8$ s$^{-1}$ and $f^+_{CH_4} \approx 1 \times 10^9$ s$^{-1}$). However, we think the main reason for the huge difference between the $J$ values of the $CO_2$ and $CH_4$ hydrates is due to the difference of the nucleation barriers of both hydrates, $\Delta G_c \sim 22 k_B T$ and $\sim 95\, k_B T$, for the $CO_2$ and $CH_4$ hydrate, respectively, as we discuss in Sec. III F.

### F. Interfacial free energy between the hydrate and the aqueous solution

It is interesting to analyze in detail the expression leading to $J$ when using CNT (which is the expression used in the Seeding technique) and particularly Eqs. (5) and (8) in the context of the $CO_2$ and $CH_4$ hydrates. It is important to recall again that the comparison between $J$ values for both hydrates is performed at the same pressure (400 bar) and supercooling ($\Delta T = 35$ K). According to Eq. (5), $J$ is given by the product of a kinetic prefactor, $J_0$, and a free energy barrier within an exponential term. The comparison of $J_0$ for $CH_4$ and $CO_2$ hydrates shows that they are quite similar. They only differ in one order of magnitude but we must explain 30 orders of magnitude of difference. The Zeldovich factor of the $CO_2$ hydrate is twice that of methane, but the attachment rate is one-half so that the product of $Z$ and $f^+$ are almost identical in both cases. The density of the gas in the liquid phase is about one order of magnitude larger for $CO_2$ than for $CH_4$ (due to its higher solubility in water). Thus, the higher solubility of $CO_2$ in water affects the prefactor $J_0$ (in the expression of $J$) by only one order of magnitude. Therefore, differences must come from the exponential free energy barrier, which has two components, $\Delta\mu_N$ and $N_c$. For $S = 1$, $\Delta\mu_N$ amounts to $-2.26$ and $-2.42 k_B T$ for the $CO_2$ and $CH_4$ hydrates, respectively. This goes in the right direction, as for a certain fixed value of $N_c$, the free energy barrier will be smaller for $CO_2$ than for $CH_4$. However, the difference does not seem so large to explain the difference in the nucleation rate. The difference in the nucleation rate comes from $N_c$, which contains 83 molecules of methane but only 20 of $CO_2$ under the same conditions. This is the key to understanding the differences: the critical cluster of the $CO_2$ hydrate is much smaller than that of the $CH_4$ hydrate. To analyze the physical origin of the difference, let us consider Eq. (3), which describes the critical cluster size. The values of $\rho_s$ and $\Delta\mu_N$ are quite similar for both hydrates; therefore, the key for the different behaviors must be on the value of the interfacial free energy $\gamma$ that moreover appears elevated to the third power.

According to de Hijes *et al.*,[100] $\gamma$ should vary linearly with $1/r_c$. Particularly, they have found this relationship for several systems including the hard-sphere and Lennard-Jones simplified models as well as more sophisticated force fields for water as the mW and TIP4P/Ice. This allows us to estimate the interfacial free energy of the corresponding planar solid–fluid interface from the knowledge of two values of $\gamma$ associated with two different critical $CO_2$ hydrate clusters. For further details, we refer to the reader to Fig. 2 of the work of de Hijes *et al.*[100] Using Eq. (3), one can calculate the values of $\gamma$ as a function of the critical cluster radius for systems with $S = 1$ and $S = 1.207$ at $T = 255$ K and 400 bar and with these values extrapolate $\gamma$ to the planar interface ($r_c \to \infty$), as shown in Fig. 12. For $S = 1$, the value of $\gamma$ for the $CO_2$ system is around 19 mJ/m$^2$, and the extrapolation to the hydrate–water planar interface yields 22.3 mJ/m$^2$. Notice that this value of the planar interface is not at the three-phase coexistence point but at the two-phase (hydrate-liquid) equilibrium at 250 K and 400 bar for the planar interface. See Fig. 13 of our last work on nucleation.[27] However, for the $CH_4$ hydrate, the value of $\gamma$ is of about 32 mJ/m$^2$ when $S = 1$ and of about 39 mJ/m$^2$ for the planar hydrate–water interface. Thus, the higher nucleation rate of $J$ for the $CO_2$ hydrate compared to the $CH_4$ hydrate arises from a lower value of $\gamma$ that significantly decreases the free energy barrier. Although it is almost impossible to present a molecular explanation,

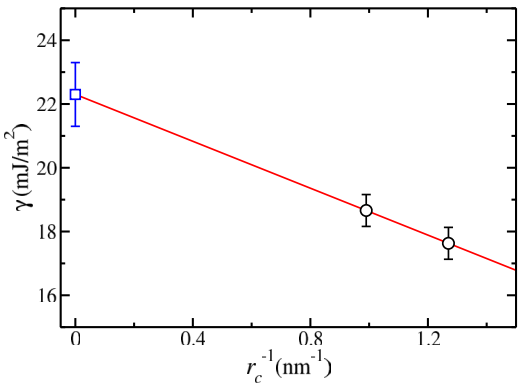


**FIG. 12.** $CO_2$ hydrate–solution interfacial free energy, $\gamma$, as a function of the inverse critical radius $r_c$ at 255 K and 400 bar. The black circles represent the values found with Seeding for supersaturations $S = 1$ (left) and $S = 1.207$ (right). These values are obtained using the $\bar{q}_3 - \bar{q}_{12}$ linear combination shown in Fig. 3 to get the number of molecules in the cluster. The red line corresponds to a linear fit of the $\gamma$ values obtained from Seeding. The blue square represents the extrapolated value of $\gamma$ (22.3 mJ/m$^2$) obtained as $r_c \to \infty$ (planar interface).

one could argue that when the composition of the fluid phase is more similar to that of the hydrate (which has a molar fraction of the gas molecule of 8/54 = 0.148), the interfacial free energy becomes smaller. The higher values of $\gamma$ for the $CH_4$ hydrate–water interface would arise from a larger difference in composition between the aqueous phase and the hydrate. Thus, the higher solubility of $CO_2$ in water would affect the nucleation rate not in the kinetic prefactor, which only contributes to the difference in one order of magnitude, nor in the value of $\Delta\mu_N$ but on decreasing significantly the value of $\gamma$.

There is an additional interesting observation. The value of $\gamma$ of the hydrate–water planar interface for the $CO_2$ systems seems to increase with temperature along the two-phase coexistence line. In fact, for 255 K, the estimated value is 22 mJ/m$^2$, whereas $\gamma$ is around 30(2) mJ/m$^2$ at $T_3$ = 290 K at this pressure according to previous calculations by some of us using the mold integration host and guest methodology.[84,85]

It is also useful to inspect the density profiles of $CO_2$ and water at the $CO_2$ hydrate–water interface and to compare to those corresponding to the $CH_4$ hydrate–water interface. Figure 13 shows the density profiles of water and $CH_4$ molecules in panel (a) and of water and $CO_2$ in panel (b). The results were obtained in our previous studies.[67,72] It should be noted that results for the $CO_2$ hydrate were already presented in Fig. 6 of the work of Algaba *et al.*[72] In both cases, the results were obtained from anisotropic *NPT* simulations at 400 bar and temperatures ranging from 250 to 295 K. As can be observed, the profiles of $CO_2$ and water in the hydrate phase and near the interface, shown in panel (b), exhibit the usual behavior expected in solid–fluid coexistence. It should be noted that the density profiles of $CH_4$ and water near the corresponding interface, presented in panel (a), show the same structural order due to the presence of the hydrate phase. There are some differences in behavior between the excess concentration of $CO_2$ on the surface compared to $CH_4$. First, we can see that the outward-most peaks of the two hydrate phases (at around 3–3.5 nm) are rather different, with the peak for $CO_2$ being broader. Second, there is a "tail" for the $CO_2$ profiles, which decay significantly slower than the $CH_4$ case. The tail of the $CO_2$ distributions stabilizes only between 4 and 4.5 nm. The results of Fig. 13 seem to suggest an excess of $CO_2$ at the water–hydrate interface (although the rigorous determination of the adsorption of the gas at the hydrate–water interface is left to future work). This may provide a mechanism that further decreases the free energy between the hydrate and the $CO_2$ aqueous solution.

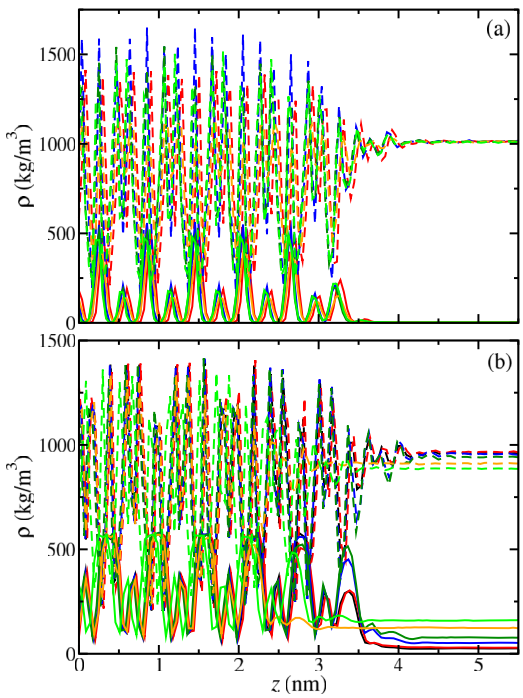


**FIG. 13.** Simulated equilibrium density profiles of methane and carbon dioxide (continuous curves in both panels) and water (dashed curves), $\rho(z)$, across the hydrate–liquid interface as obtained from MD anisotropic *NPT* simulations at 400 bar and 250 (black), 260 (red), 270 (blue), 280 (dark green), 290 (orange), and 295 K (light green). Panel (a) corresponds to the $CH_4$ hydrate–liquid interface and panel (b) to the $CO_2$ hydrate–liquid interface.

Finally, it would be interesting in this context to estimate the empty hydrate–water interfacial free energy to compare to the values obtained here and in previous studies[72,84–86] for the $CH_4$ and $CO_2$ hydrates. However, empty structures of hydrates, including sI, sII, and sH, are usually called virtual ices. According to Conde *et al.*,[101] the empty hydrates sII and sH appear to be the stable solid phases of water at negative pressures. Consequently, the sI and other virtual ices do not enter the phase diagram, as shown in Fig. 5 of the work of Conde *et al.*[101] In other words, no pressure or temperature conditions exist under which these structures have lower chemical potential than $I_h$, sII, or sH crystallographic structures. Thus, there is a high risk for the growth of another phase of ice from a template of sI (using, for instance, the mold integration technique[84,102,103]) and that would prevent the determination of the value of $\gamma$ for the sI–water interface. This issue should be examined in greater detail in future work.

### G. Nucleation along the $S$ = 1 curve

The value of $J$ at 255 K for $S$ = 1 is of the order of $10^{25}/(\mathrm{m}^3\ \mathrm{s})$. Nucleation can be observed spontaneously in BF runs when the nucleation rate is larger than $10^{29}/(\mathrm{m}^3\ \mathrm{s})$ with the current computational resources. Therefore, it seems likely that nucleation can be observed in BF runs at $S = 1$ if we move to lower temperatures (thus increasing the driving force). This is of particular interest as nucleation studies in experiments are usually performed along the $S = 1$ curve (with the solution in contact with a gas reservoir[104]).

We performed BF runs at 245 and 250 K (and 400 bar) at the corresponding $CO_2$ saturation concentration. These states are represented as red diamonds in Fig. 1 (note that they are located on the $S = 1$ red line). The details on these simulations are given in Table III. As we have already mentioned, we used two types of simulation setups for this study: a homogeneous $CO_2$ saturated bulk solution (denoted as "one-phase system" in Table III) and a saturated solution in contact with a fluid $CO_2$ reservoir (denoted as "two-phase system" in Table III). We focus first on the one-phase system and analyze later on the comparison between both setups. We used isotropic *NPT* runs for the one-phase systems. As

**TABLE III.** Simulation details and results obtained using BF simulations at 250 and 245 K, both at 400 bar and supersaturation $S = 1$ in one- and two-phase systems.

| | One-phase system | Two-phase system |
|---|---|---|
| $T$ (K) | 250 | |
| $N^{H_2O}$ | 6524 | 7200 |
| $N^{CO_2}$ | 606 | 3444 |
| $x_{CO_2}$ | 0.085 | 0.085 |
| Box dim. ($nm^3$) | $6.06 \times 6.06 \times 6.06$ | $9.07 \times 6.25 \times 7.41$ |
| Liquid dim. ($nm^3$) | $6.06 \times 6.06 \times 6.06$ | $5.77 \times 6.25 \times 7.41$ |
| $V_{liq}$ ($nm^3$) | 222 | 267 |
| $n_{runs}$ | 12 | 12 |
| $n_{nucl}$ | 4 | 4 |
| $t_{nucl}$ (ns) | 730 | 245 |
| | 1310 | 285 |
| | 1570 | 480 |
| | 1700 | 1510 |
| $t_{total}$ (ns) | 21 310 | 18 520 |
| $\rho_L^{CO_2}$ ($m^{-3}$) | $2.7 \times 10^{27}$ | $2.7 \times 10^{27}$ |
| $J$ ($m^{-3}\ s^{-1}$) | $8.45 \times 10^{29}$ | $8.09 \times 10^{29}$ |
| $T$ (K) | 245 | |
| $N^{H_2O}$ | 2400 | 2400 |
| $N^{CO_2}$ | 240 | 1148 |
| $x_{CO_2}$ | 0.09 | 0.09 |
| Box dim. ($nm^3$) | $4.35 \times 4.35 \times 4.35$ | $9.19 \times 6.25 \times 2.47$ |
| $V_{liq}$ ($nm^3$) | 82.5 | 82.5 |
| $n_{runs}$ | 2 | 2 |
| $n_{nucl}$ | 2 | 2 |
| $t_{nucl}$ (ns) | 640 | 300 |
| | 550 | 230 |
| $t_{total}$ (ns) | 1190 | 530 |
| $\rho_L^{CO_2}$ ($m^{-3}$) | $2.9 \times 10^{27}$ | $2.9 \times 10^{27}$ |
| $J$ ($m^{-3}\ s^{-1}$) | $2.02 \times 10^{31}$ | $5.78 \times 10^{31}$ |

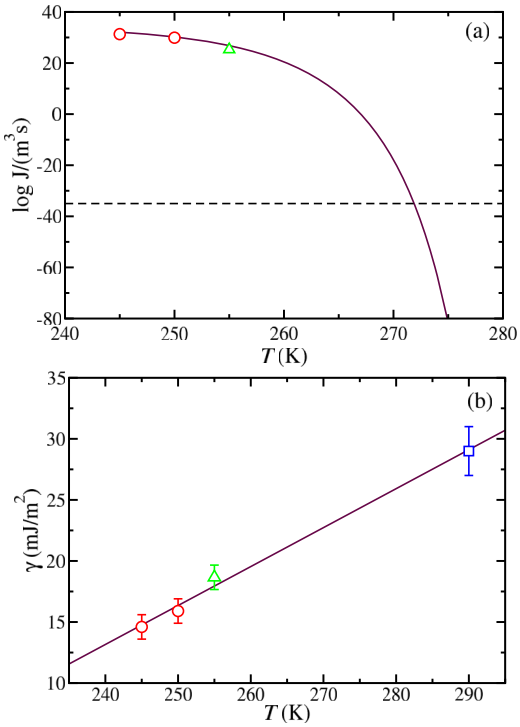


**FIG. 14.** $CO_2$ hydrate nucleation rate, $J$, (a) and $CO_2$ hydrate–water interfacial free energy, $\gamma$, (b), as functions of temperature along the $S = 1$ curve. The red circles and green triangles are BF and Seeding results obtained in this work, respectively. The blue square is the $CO_2$ hydrate–water interfacial free energy under coexistence conditions obtained by Algaba *et al.*[84] through mold integration.[102] Continuous curve in panel (a) is obtained using simulation data via the CNT approach and line in panel (b) is a linear fit of simulation data. The curve of $J$ as a function of time is obtained using the $\gamma(T)$ dependence found in panel (b). The dashed horizontal line in panel (a) corresponds to an "unachievable" nucleation rate given by one nucleus per universe age and hydrosphere volume.



not all trajectories were successful in nucleating the solid phase, we used the method of Walsh *et al.*,[49] described previously in the manuscript when discussing the BF runs for $S = 1.207$, to determine the nucleation rate. We obtain a nucleation rate of the order of $10^{31}/(m^3\ s)$ for 245 K and of $10^{29}/(m^3\ s)$ for 250 K. These nucleation rates are fully consistent with the $J = 10^{25}\ m^{-3}\ s^{-1}$ obtained in this work for $S = 1$ at 255 K via Seeding (see Sec. III E). The $J$ values obtained from BF simulations along the $S = 1$ line (red circles) are compared to that obtained via Seeding for $S = 1$ (green triangle) in Fig. 14(a).

In the following sections, we describe how we combine our nucleation studies at $S = 1$ and three different temperatures (245, 250, and 255 K) with a recent calculation of $\gamma$ between the solid and the solution at the three-phase coexistence temperature[84] to get an estimate of the whole $J(T)$ curve along the $S = 1$ line.

### 1. $\gamma$ along $S = 1$

To estimate $J$ along $S = 1$, we first need to know how $\gamma$ varies along $S = 1$, given that the nucleation barrier can be obtained from $\gamma$ through Eq. (4). We already have a value of $\gamma$ from Seeding at $S = 1$ and 255 K [18.7 $mJ/m^2$, depicted with a green triangle in Fig. 14(b)]. Recently, some of us estimated $\gamma$ at $T_3$ (the temperature where solid, solution and $CO_2$ reservoir coexists,[84] indicated by an maroon circle in Fig. 1 for $S = 1$). The value found was 29(2) $mJ/m^2$ at 287 K. The $T_3$ value was later refined to 290 K.[72] We assume here that the value of $\gamma$ found in the work of Algaba and collaborators[84] at 287 K is valid for the updated $T_3$ of 290 K (the temperature difference between both $T_3$ estimates is small). The value of $\gamma$ at $T_3$ is represented by the blue square in Fig. 14(b).

We now try to get an estimate of $\gamma$ from the two BF simulation studies performed at 245 and 250 K. To do that, we use Eq. (5) to get $\Delta G_c$ from $J$ and, then, Eq. (4) to obtain $\gamma$ from $\Delta G_c$ (the $CO_2$ density in the solid phase used for these calculations is $\rho_S^{CO_2} = 4.7 \times 10^{27}\ m^{-3}$ for both temperatures). The first of these two steps requires an estimate of $J_0$. To estimate $J_0$, we need $f^+$. We use the fact that $f^+$ is proportional to the $CO_2$ diffusion coefficient, $D_{CO_2}$, and to $N_c^{2/3}$,[23] to obtain $f^+$ at 245 and 250 K from the $f^+$ calculated at 255 K. This requires computing $D_{CO_2}$ at 245,

250, and 255 K and estimating $N_c$ in the BF runs. The $CO_2$ diffusion coefficients that we get from *NPT* simulations of the aqueous solutions are 1.6, 2.2, and 3.0 × $10^{-11}$ $m^{-2}$ $s^{-1}$ for 245, 250, and 255 K, respectively. To estimate $N_c$, we identify the largest cluster that appears during the induction period previous to hydrate growth (see Fig. 15). In this way, we get 42 and 95 water molecules in the critical cluster at 245 and 250 K, respectively, which are values fully consistent with $N_c^{H_2O}$ = 115 obtained with Seeding at 255 K. While this estimate of $N_c$ might not be accurate, the final value of $\gamma$ is not significantly influenced by this inaccuracy, as we argue further on. The $|\Delta\mu_N|$ factor in $J_0$ is taken from our previous work using route 4.[72] We get $|\Delta\mu_N|$ = 2.98 and 2.59$k_BT$ at 245 and 250 K, respectively. With these ingredients, we obtain the $\gamma$ estimates represented in Fig. 14(b) by the red circles (14.6 and 16.0 mJ/$m^2$ at 245 and 250 K respectively).

The $\gamma$ estimates from BF simulations (red circles), from Seeding simulations (green triangles), and from mold integration (blue square) are fully consistent among each other and can be fitted quite nicely to a straight line (maroon line). $\gamma$ increases with temperature along the $S$ = 1 line roughly at a rate of 1 mJ/$m^2$ every 3 K.

Interestingly, BF simulations yield a $\gamma$ value less sensitive to the order parameter than the Seeding method. In Seeding, Eq. (3) is used to infer $\gamma$ from the $N_c$ value obtained in seeded simulations, which has a strong dependence on the chosen order parameter. In contrast, in the BF approach, $N_c$ is used for estimating the kinetic pre-factor. As the natural logarithm of this pre-factor is taken to calculate $\Delta G_c$ [from which $\gamma$ is then obtained via Eq. (4)], the influence of $N_c$ on the final $\gamma$ value is relatively minor. To illustrate this, let us consider the impact of doubling the cluster size in the calculation of $\gamma$. In Seeding (255 K), $\gamma$ would significantly increase from 18.7 to 23.5 mJ/$m^2$. However, in BF simulations, the changes are much smaller: from 14.6 to 14.9 mJ/$m^2$ at 245 K, and from 16.0 to 16.2 mJ/$m^2$ at 250 K. In conclusion, (i) BF simulations provide an estimate of $\gamma$ less influenced by the choice of order parameter than Seeding; (ii) the way in which we obtain $N_c$ from BF simulations is good enough to get a reliable estimate of $\gamma$.

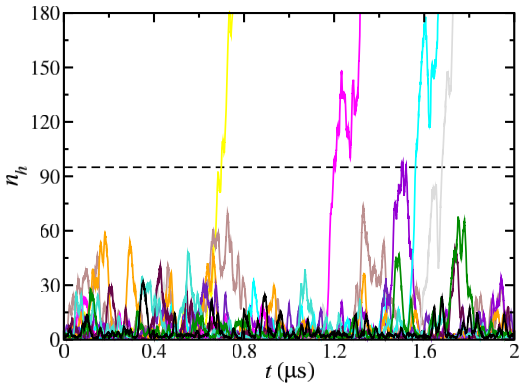


**FIG. 15.** Number of water molecules in the largest cluster of the $CO_2$ hydrate, $n_h$, as a function of time, for different bulk simulations at $S$ = 1 and 250 K. $CO_2$ hydrate growth is observed in four trajectories. The dashed horizontal line, which highlights the largest sub-critical cluster that emerged in all simulations, is our estimate for $N_c^{H_2O}$ using the $\bar{q}_3 - \bar{q}_{12}$ linear combination of the local bond order parameters (95 in the present example).

### 2. J along S = 1

Using the linear fit of $\gamma(T)$ shown in Fig. 14(b), we can obtain $\Delta G_c$ at any temperature using Eq. (5) with the $|\Delta\mu_N|$ obtained in our previous work (route 4).[72] We use the following fit for the chemical potential difference: $|\Delta\mu_N|/(k_BT) = -3.02 \times 10^{-4}T^2 + 0.228T - 40.7$. With $\Delta G_c$ and Eq. (8), we can estimate $J$ at any temperature, provided that we have $J_0$ as well. This requires having $f^+$ at any $T$ [see Eq. (5)]. For that purpose, we again use the fact that $f^+ \propto N_c^{2/3} D_{CO_2}$.[23] On the one hand, through *NPT* simulations of the saturated aqueous solution at different temperatures, we got the following fit to obtain $D_{CO_2}$ at any temperature: $\ln[D/(m^2/s)] = -0.0011T^2 + 0.6846T - 124.99$. On the other hand, $N_c$ can be obtained at any $T$ using $\Delta G_c = N_c|\Delta\mu|/2$ according to Eq. (2). The missing factors to complete the calculation of $J_0$ (and of $J$) are the Zeldovich factor $Z$, which can be easily computed through $N_C$ and $|\Delta\mu_N|$ [Eq. (6)], and $\rho_L^{CO_2}$, which is trivially obtained in *NPT* simulations. With these ingredients, we can draw the maroon curve in Fig. 14(a) that predicts the trend of the nucleation rate at $S$ = 1.

Unfortunately, to the best of our knowledge, there is no experimental data to compare these simulation predictions with. In homogeneous ice nucleation, rates of the order of $10^2$ – $10^{16}$ $m^{-3}$ $s^{-1}$ (with microdroplets) and higher (with nanodroplets) are experimentally accessible.[105] Our predictions indicate that such rates occur at temperatures below 266 K (beyond 25 K supercooling). Therefore, we hope that simulations and experiments of homogeneous hydrate nucleation can be compared in the future, as they were for the case of ice nucleation.[105]

### 3. Bulk vs surface nucleation

The dashed horizontal line in Fig. 14(a) indicates the order of magnitude of an unachievable nucleation rate: that corresponding to 1 nucleus formed in the volume of the hydrosphere and in the age of the universe. Our CNT fit (maroon curve) predicts that this unattainable rate occurs at about 272 K (around 20 K below $T_3$). Therefore, any crystallization event at a supercooling lower than 20 K must be heterogeneous (the difficulty of observing homogeneous nucleation was also highlighted in a simulation study of methane hydrates).[20] In most experiments, hydrate crystallization typically occurs at supercooling conditions of less than 20 K.[41,106,107] Such low supercooling suggests that the nucleation of hydrates is not homogeneous in the real world. Although experiments do not provide molecular insight into the nucleation step, it is commonly believed that nucleation occurs at the gas–solution interface, perhaps assisted by impurities, the glass–solution contact line,[108] or aided by an increased concentration of the hydrate formed near the interface.[109]

To investigate the latter hypothesis, we compare BF simulation runs at 245 and 250 K performed in two-phase systems (where the solution is in contact with a $CO_2$ reservoir) to those run in one-phase systems that have been already presented (without a bulk aqueous solution having the equilibrium $CO_2$ saturation concentration). In the two-phase simulations, the details of which are reported in Table III, we used $NP_z\mathscr{A}T$ runs. Obviously, the volume used to calculate the nucleation rate is only that of the aqueous phase in two-phase systems. As reported in Table III, both simulation setups give the same nucleation rate for both temperatures (within less than half

an order of magnitude). Therefore, the $CO_2$–solution interface does not have any effect on hydrate nucleation, at least at 245 and 250 K. However, there could be a crossover between homogeneous and heterogeneous nucleation as the temperature increases (as is the case for crystallization of hard spheres with density),[110] which could explain nucleation events at low supercooling. More research is needed to identify the nucleation path in mild supercooling conditions, where hydrate formation is experimentally observed.

## IV. CONCLUSIONS

In this work, we have calculated the homogeneous nucleation rate of $CO_2$ hydrate at 400 bar and 255 K (35 K of supercooling) using classical nucleation theory and Seeding simulations. For supersaturated systems (i.e., $S = 1.207$ and $S = 1.268$), the nucleation rate can be obtained from BF simulations. Since the results of Seeding depend on the choice of the order parameter, we tested that a combination of $\bar{q}_3$ and $\bar{q}_{12}$ is able to distinguish in an efficient way the molecules of water belonging to the liquid or to the hydrate with a mislabeling of about 0.02%. By using this combination of order parameters in Seeding runs with $S = 1.207$, we confirmed that it provides an estimate of $J$ in full agreement with that obtained from BF runs. In other words, the selected order parameter allows a satisfactory estimate of the radius of the solid critical cluster at the surface of tension.

After checking the adequacy of the order parameter, we implemented the Seeding technique (in a system having two phases) for $S = 1$ at 255 K and 400 bar. We obtained a size of 115 molecules of water for the critical cluster and a value of $10^{25}/(\mathrm{m}^3\ \mathrm{s})$ for the nucleation rate. This is about 30 orders of magnitude larger than the value obtained in our previous work for methane hydrate at the same pressure and supercooling. The higher solubility of $CO_2$ is not sufficient to explain such an enormous difference. We identify that the key is a much lower value of $\gamma$ for the $CO_2$ hydrate–water interface when compared to that of the $CH_4$ hydrate–water interface, and speculate that the value of $\gamma$ in these systems could be lower when the composition of the solution becomes closer to the composition of the hydrate. The interfacial free energy of the $CO_2$ hydrate at $S = 1$ was of about 19 $\mathrm{mJ/m^2}$ compared to the value of 29 $\mathrm{mJ/m^2}$ obtained in our previous work for the methane hydrate. This means that at the same supercooling, the nucleation rate of $CO_2$ hydrate is 30 orders of magnitude higher than the estimation found in our last work of nucleation rate of methane hydrate[27] and 20 orders of magnitude higher than the nucleation rate of ice $I_h$, which at this pressure and supercooling is of around $J_{I_h} = 10^5/(\mathrm{m}^3\ \mathrm{s})$.[111]

We found that the energy required to create the planar hydrate–liquid interface is $\gamma = 22.3\ \mathrm{mJ/m^2}$ at 255 K and 400 bar, which suggests that the interfacial free energy for a planar interface should increase as the system moves along the two-phase curve from this supercooling temperature to $T_3$, where $\gamma$ is around $30(2)\ \mathrm{mJ/m^2}$ according to experiments[112–115] and our previous calculations using the mold integration host and guest methodology.[84,85]

Finally, we have shown that BF runs in a two-phase system can indeed be performed to nucleate the hydrate at 245 and 250 K to obtain $J$ when $S = 1$ at these temperatures. Comparison of the value of $J$ from simulations using two phases with a system having just one phase reveals that the water–$CO_2$ interface does not enhance the nucleation rate so that at least for temperatures below 255 K, the nucleation is homogeneous and there is not an enhancement of the nucleation rate due to heterogeneous nucleation at the water–$CO_2$ interface. However, there could be a crossover to heterogeneous nucleation at higher temperatures so that it is the main path to nucleation when closer to the equilibrium temperature $T_3$. Finally, we estimate the value of $J$ along the $S = 1$ curve, concluding that homogeneous nucleation could indeed be determined experimentally at this pressure for supercooling greater than 25 K. Our simulations predict that homogeneous nucleation is not viable for supercooling lower than 20 K. Therefore, nucleation must be heterogeneous in typical experiments where hydrate formation is observed at low supercooling.

## ACKNOWLEDGMENTS

This work was financed by Ministerio de Ciencia e Innovación (Grant Nos. PID2021-125081NB-I00 and PID2024-158030NB-I00), Junta de Andalucía (Grant No. P20-00363), and Universidad de Huelva (Grant Nos. P.O. FEDER UHU-1255522, FEDER-UHU-202034, and EPIT1282023), all six co-financed by EU FEDER funds. We acknowledge the RES resources provided by the Barcelona Supercomputing Center in Mare Nostrum under Grant No. FI-2023-2-0041. The authors also acknowledge Project No. PID2019-105898GB-C21 of the Ministerio de Educación y Cultura. We also acknowledge access to supercomputer time from RES from Project No. FI-2022-1-0019. J.G. acknowledges Polish high-performance computing infrastructure PLGrid (HPC Center: ACK Cyfronet AGH) for providing computer facilities and support under computational Grant No. PLG/2024/017195. Part of the computations was carried out at the Centre of Informatics Tricity Academic Supercomputer and Network. C. Vega, E. Sanz, and S. Blazquez acknowledge the funding from Project No. PID2022-136919NB-C31 of Ministerio de Ciencia e Innovacion.

## AUTHOR DECLARATIONS

### Conflict of Interest

The authors have no conflicts to disclose.

### Author Contributions

**I. M. Zerón**: Conceptualization (equal); Data curation (lead); Formal analysis (lead); Investigation (equal); Methodology (equal); Supervision (equal); Writing – original draft (equal); Writing – review & editing (equal). **J. Algaba**: Conceptualization (lead); Data curation (equal); Formal analysis (lead); Investigation (equal); Methodology (equal); Writing – original draft (equal); Writing – review & editing (equal). **J. M. Míguez**: Conceptualization (equal); Data curation (equal); Investigation (equal); Methodology (equal); Writing – review & editing (equal). **J. Grabowska**: Conceptualization (equal); Data curation (equal); Investigation (equal); Methodology (equal); Writing – review & editing (equal). **S. Blazquez**: Investigation (equal); Methodology (equal); Writing – review & editing (equal). **E. Sanz**: Investigation (equal); Methodology (equal); Writing – review & editing (equal). **C. Vega**: Conceptualization (equal); Investigation (equal); Methodology (equal); Writing – review & editing (equal). **F. J. Blas**: Conceptualization (lead); Investigation (lead);

Methodology (equal); Supervision (equal); Writing – original draft (equal); Writing – review & editing (equal).

## DATA AVAILABILITY

The data that support the findings of this study are available within the article.

## REFERENCES


[1] P. G. Debenedetti, *Metastable Liquids: Concepts and Principles* (Princeton University Press, 2020).

[2] C. A. Stan, G. F. Schneider, S. S. Shevkoplyas, M. Hashimoto, M. Ibanescu, B. J. Wiley, and G. M. Whitesides, "A microfluidic apparatus for the study of ice nucleation in supercooled water drops," Lab Chip **9**, 2293–2305 (2009).

[3] P. Taborek, "Nucleation in emulsified supercooled water," Phys. Rev. B **32**, 5902 (1985).

[4] P. J. DeMott and D. C. Rogers, "Freezing nucleation rates of dilute solution droplets measured between −30° and −40 °C in laboratory simulations of natural clouds," J. Atmos. Sci. **47**, 1056–1064 (1990).

[5] P. Stöckel, I. M. Weidinger, H. Baumgärtel, and T. Leisner, "Rates of homogeneous ice nucleation in levitated $H_2O$ and $D_2O$ droplets," J. Phys. Chem. A **109**, 2540–2546 (2005).

[6] B. Krämer, O. Hübner, H. Vortisch, L. Wöste, T. Leisner, M. Schwell, E. Rühl, and H. Baumgärtel, "Homogeneous nucleation rates of supercooled water measured in single levitated microdroplets," J. Chem. Phys. **111**, 6521–6527 (1999).

[7] D. Duft and T. Leisner, "Laboratory evidence for volume-dominated nucleation of ice in supercooled water microdroplets," Atmos. Chem. Phys. **4**, 1997–2000 (2004).

[8] H. Laksmono, T. A. McQueen, J. A. Sellberg, N. D. Loh, C. Huang, D. Schlesinger, R. G. Sierra, C. Y. Hampton, D. Nordlund, M. Beye *et al.*, "Anomalous behavior of the homogeneous ice nucleation rate in 'no-man's land'," J. Phys. Chem. Lett. **6**, 2826–2832 (2015).

[9] A. Manka, H. Pathak, S. Tanimura, J. Wölk, R. Strey, and B. E. Wyslouzil, "Freezing water in no-man's land," Phys. Chem. Chem. Phys. **14**, 4505–4516 (2012).

[10] D. E. Hagen, R. J. Anderson, and J. L. Kassner, Jr., "Homogeneous condensation—Freezing nucleation rate measurements for small water droplets in an expansion cloud chamber," J. Atmos. Sci. **38**, 1236–1243 (1981).

[11] R. C. Miller, R. J. Anderson, J. L. Kassner, Jr., and D. E. Hagen, "Homogeneous nucleation rate measurements for water over a wide range of temperature and nucleation rate," J. Chem. Phys. **78**, 3204–3211 (1983).

[12] G. M. Torrie and J. P. Valleau, "Nonphysical sampling distributions in Monte Carlo free-energy estimation: Umbrella sampling," J. Comput. Phys. **23**, 187–199 (1977).

[13] A. Laio and M. Parrinello, "Escaping free-energy minima," Proc. Natl. Acad. Sci. U. S. A. **99**, 12562–12566 (2002).

[14] M. Volmer and A. Weber, "Keimbildung in übersättigten gebilden," Z. Phys. Chem. **119U**, 277–301 (1926).

[15] R. Becker and W. Döring, "Kinetische behandlung der keimbildung in übersättigten dämpfen," Ann. Phys. **416**, 719–752 (1935).

[16] P. G. Bolhuis, D. Chandler, C. Dellago, and P. L. Geissler, "TRANSITION PATH SAMPLING: Throwing ropes over rough mountain passes, in the dark," Annu. Rev. Phys. Chem. **53**, 291 (2002).

[17] Y. Bi and T. Li, "Probing methane hydrate nucleation through the forward flux sampling method," J. Phys. Chem. B **118**, 13324 (2014).

[18] A. Haji-Akbari and P. G. Debenedetti, "Direct calculation of ice homogeneous nucleation rate for a molecular model of water," Proc. Natl. Acad. Sci. U. S. A. **112**, 10582–10588 (2015).

[19] E. Sanz, C. Vega, J. R. Espinosa, R. Caballero-Bernal, J. L. F. Abascal, and C. Valeriani, "Homogeneous ice nucleation at moderate supercooling from molecular simulation," J. Am. Chem. Soc. **135**, 15008–15017 (2013).

[20] B. C. Knott, V. Molinero, M. F. Doherty, and B. Peters, "Homogeneous nucleation of methane hydrates: Unrealistic under realistic conditions," J. Am. Chem. Soc. **134**, 19544–19547 (2012).

[21] X.-M. Bai and M. Li, "Test of classical nucleation theory via molecular-dynamics simulation," J. Chem. Phys. **122**, 224510 (2005).

[22] X.-M. Bai and M. Li, "Calculation of solid-liquid interfacial free energy: A classical nucleation theory based approach," J. Chem. Phys. **124**, 124707 (2006).

[23] J. R. Espinosa, C. Vega, C. Valeriani, and E. Sanz, "Seeding approach to crystal nucleation," J. Chem. Phys. **144**, 034501 (2016).

[24] J. R. Espinosa, C. Vega, C. Valeriani, and E. Sanz, "The crystal-fluid interfacial free energy and nucleation rate of NaCl from different simulation methods," J. Chem. Phys. **142**, 194709 (2015).

[25] J. R. Espinosa, E. Sanz, C. Valeriani, and C. Vega, "Homogeneous ice nucleation evaluated for several water models," J. Chem. Phys. **141**, 18C529 (2014).

[26] G. D. Soria, J. R. Espinosa, J. Ramirez, C. Valeriani, C. Vega, and E. Sanz, "A simulation study of homogeneous ice nucleation in supercooled salty water," J. Chem. Phys. **148**, 222811 (2018).

[27] J. Grabowska, S. Blázquez, E. Sanz, E. G. Noya, I. M. Zerón, J. Algaba, J. M. Míguez, F. J. Blas, and C. Vega, "Homogeneous nucleation rate of methane hydrate formation under experimental conditions from seeding simulations," J. Chem. Phys. **158**, 114505 (2023).

[28] E. D. Sloan and C. Koh, *Clathrate Hydrates of Natural Gases*, 3rd ed. (CRC Press, New York, 2008).

[29] J. A. Ripmeester and S. Alavi, *Clathrate Hydrates: Molecular Science and Characterization* (Wiley VCH, Weinheim, Germany, 2022).

[30] Z.-c. Zhang, N.-y. Wu, C.-l. Liu, X.-l. Hao, Y.-c. Zhang, K. Gao, B. Peng, C. Zheng, W. Tang, and G.-j. Guo, "Molecular simulation studies on natural gas hydrates nucleation and growth: A review," China Geol. **5**, 330–344 (2022).

[31] J. A. Ripmeester and S. Alavi, "Some current challenges in clathrate hydrate science: Nucleation, decomposition and the memory effect," Curr. Opin. Solid State Mater. Sci. **20**, 344–351 (2016).

[32] R. E. Pellenbarg, M. D. Max, and S. M. Clifford, "Methane and carbon dioxide hydrates on Mars: Potential origins, distribution, detection, and implications for future in situ resource utilization," J. Geophys. Res.:Planets **108**, 8042, https://doi.org/10.1029/2002je001901 (2003).

[33] N. J. English and J. M. D. MacElroy, "Perspectives on molecular simulation of clathrate hydrates: Progress, prospects and challenges," Chem. Eng. Sci. **121**, 133–156 (2015).

[34] H. Tanaka, M. Matsumoto, and T. Yagasaki, "Efficiency and energy balance for substitution of $CH_4$ in clathrate hydrates with $CO_2$ under multiple-phase coexisting conditions," J. Chem. Phys. **159**, 194504 (2023).

[35] K. Lekvam and P. Ruoff, "A reaction kinetic mechanism for methane hydrate formation in liquid water," J. Am. Chem. Soc. **115**, 8565–8569 (1993).

[36] S. Devarakonda, A. Groysman, and A. S. Myerson, "THF–water hydrate crystallization: An experimental investigation," J. Cryst. Growth **204**, 525 (1999).

[37] S. Takeya, A. Hori, T. Hondoh, and T. Uchida, "Freezing-memory effect of water on nucleation of $CO_2$ hydrate crystals," J. Phys. Chem. B **104**, 4164 (2000).

[38] J. M. Herri, J. S. Pic, F. Gruy, and M. Cournil, "Methane hydrate crystallization mechanism from *in-situ* particle sizing," AIChE J. **45**, 590 (2004).

[39] H. K. Abay and T. M. Svartaas, "Multicomponent gas hydrate nucleation: The effect of the cooling rate and composition," Energy Fuels **25**, 42 (2010).

[40] L. Jensen, K. Thomsen, and N. von Solms, "Propane hydrate nucleation: Experimental investigation and correlation," Chem. Eng. Sci. **63**, 3069 (2008).

[41] N. Maeda, "Nucleation curves of methane hydrate from constant cooling ramp methods," Fuel **223**, 286 (2018).

[42] N. Maeda and X. d. Shen, "Scaling laws for nucleation rates of gas hydrate," Fuel **253**, 1597 (2019).

[43] L. A. Báez and P. Clancy, "Computer simulation of the crystal growth and dissolution of natural gas hydrates," Ann. N. Y. Acad. Sci. **715**, 177 (1994).

[44] P. M. Rodger, T. R. Forester, and W. Smith, "Simulations of the methane hydrate/methane gas interface near hydrate forming conditions conditions," Fluid Phase Equilib. **116**, 326 (1996).

[45] S. Alavi, J. A. Ripmeester, and D. D. Klug, "Molecular-dynamics study of structure II hydrogen clathrates," J. Chem. Phys. **123**, 024507 (2005).

[46]S. Alavi, J. A. Ripmeester, and D. D. Klug, "Molecular-dynamics simulations of binary structure II hydrogen and tetrahydrofurane clathrates," J. Chem. Phys. **124**, 014704 (2006).
[47]M. R. Walsh, C. A. Koh, E. D. Sloan, A. K. Sum, and D. T. Wu, "Microsecond simulations of spontaneous methane hydrate nucleation and growth," Science **326**, 1095 (2009).
[48]N. J. English and J. S. Tse, "Mechanisms for thermal conduction in methane hydrate," Phys. Rev. Lett. **103**, 015901 (2009).
[49]M. R. Walsh, G. T. Beckham, C. A. Koh, E. D. Sloan, D. T. Wu, and A. K. Sum, "Methane hydrate nucleation rates from molecular dynamics simulations: Effects of aqueous methane concentration, interfacial curvature, and system size," J. Phys. Chem. C **115**, 21241 (2011).
[50]S. Sarupria and P. G. Debenedetti, "Homogeneous nucleation of methane hydrate in microsecond molecular dynamics simulations," J. Phys. Chem. Lett. **3**, 2942 (2012).
[51]S. Liang and P. G. Kusalik, "Nucleation of gas hydrates within constant energy systems," J. Phys. Chem. B **117**, 1403 (2013).
[52]B. C. Barnes, B. C. Knott, G. T. Beckham, D. T. Wu, and A. K. Sum, "Reaction coordinate of incipient methane clathrate hydrate nucleation," J. Phys. Chem. B **118**, 13236–13243 (2014).
[53]D. Yuhara, B. C. Barnes, D. Suh, B. C. knott, G. T. Beckham, K. Yasuoka, D. T. Wu, and A. K. Sum, "Nucleation rate analysis of methane hydrate from molecular dynamics simulations," Faraday Discuss. **179**, 463–474 (2015).
[54]Z. Zhang, C.-J. Liu, M. R. Walsh, and G.-J. Guo, "Effects of ensembles on methane hydrate nucleation kinetics," Phys. Chem. Chem. Phys. **18**, 15602 (2016).
[55]M. Lauricella, G. Ciccotti, N. J. English, B. Peters, and S. Meloni, "Mechanisms and nucleation rate of methane hydrate by dynamical nonequilibrium molecular dynamics," J. Phys. Chem. C **121**, 24223 (2017).
[56]Arjun, T. A. Berendsen, and P. G. Bolhuis, "Unbiased atomistic insight in the competing nucleation mechanisms of methane hydrates," Proc. Natl. Acad. Sci. U. S. A. **116**, 19305 (2019).
[57]A. Arjun and P. G. Bolhuis, "Rate prediction for homogeneous nucleation of methane hydrate at moderate supersaturation using transition interface sampling," J. Phys. Chem. B **124**, 8099 (2020).
[58]A. Arjun and P. G. Bolhuis, "Homogenous nucleation rate of $CO_2$ hydrates using transition interface sampling," J. Chem. Phys. **154**, 164507 (2021).
[59]A. Arjun and P. G. Bolhuis, "Homogeneous nucleation of crystalline methane hydrate in molecular dynamics transition paths sampled under realistic conditions," J. Chem. Phys. **158**, 044504 (2023).
[60]Z. Zhang, P. G. Kusalik, and G.-J. Guo, "Molecular insight into the growth of hydrogen and methane binary hydrates," J. Phys. Chem. C **122**, 7771–7778 (2018).
[61]Z. Zhang, G.-J. Guo, N. Wu, and P. G. Kusalik, "Molecular insights into guest and composition dependence of mixed hydrate nucleation," J. Phys. Chem. C **124**, 25078–25086 (2020).
[62]J.-L. Wang and R. J. Sadus, "Phase behaviour of binary fluid mixtures: A global phase diagram solely in terms of pure component properties," Fluid Phase Equilib. **214**, 67–78 (2003).
[63]F. Jiménez-Ángeles and A. Firoozabadi, "Nucleation of methane hydrates at moderate subcooling by molecular dynamics simulations," J. Phys. Chem. C **118**, 11310–11318 (2014).
[64]F. Jiménez-Ángeles and A. Firoozabadi, "Hydrophobic hydration and the effect of NaCl salt in the adsorption of hydrocarbons and surfactants on clathrate hydrates," ACS Cent. Sci. **4**, 820–831 (2018).
[65]H. Tanaka, M. Matsumoto, and T. Yagasaki, "On the phase behaviors of $CH_4$–$CO_2$ binary clathrate hydrates: Two-phase and three-phase coexistences," J. Chem. Phys. **158**, 224502 (2023).
[66]H. Tanaka, M. Matsumoto, and T. Yagasaki, "Cage occupancies of $CH_4$, $CO_2$, and Xe hydrates: Mean field theory and grandcanonical Monte Carlo simulations," J. Chem. Phys. **160**, 044502 (2024).
[67]J. Grabowska, S. Blázquez, E. Sanz, I. M. Zerón, J. Algaba, J. M. Míguez, F. J. Blas, and C. Vega, "Solubility of methane in water: Some useful results for hydrate nucleation," J. Phys. Chem. B **126**, 8553–8570 (2022).
[68]Z. Zhang, P. G. Kusalik, and G.-J. Guo, "Bridging solution properties to gas hydrate nucleation through guest dynamics," Phys. Chem. Chem. Phys. **20**, 24535–24538 (2018).
[69]L. Farkas, "Keimbildungsgeschwindigkeit in übersättigten dämpfen," Z. Phys. Chem. **125U**, 236–242 (1927).
[70]Y. B. Zeldovich, "On the theory of new phase formation: Cavitation," Acta Physicochem., USSR **18**, 1 (1943).
[71]D. Kashchiev and A. Firoozabadi, "Driving force for crystallization of gas hydrates," J. Cryst. Growth **241**, 220–230 (2002).
[72]J. Algaba, I. M. Zerón, J. M. Míguez, J. Grabowska, S. Blazquez, E. Sanz, C. Vega, and F. J. Blas, "Solubility of carbon dioxide in water: Some useful results for hydrate nucleation," J. Chem. Phys. **158**, 184703 (2023).
[73]D. van der Spoel, E. Lindahl, B. Hess, G. Groenhof, A. E. Mark, and H. J. C. Berendsen, "GROMACS: Fast, flexible, and free," J. Comput. Chem. **26**, 1701–1718 (2005).
[74]B. Hess, C. Kutzner, D. van der Spoel, and E. Lindahl, "GROMACS 4: Algorithms for highly efficient, load-balanced, and scalable molecular simulation," J. Chem. Theory Comput. **4**, 435–447 (2008).
[75]M. A. Cuendet and W. F. van Gunsteren, "On the calculation of velocity-dependent properties in molecular dynamics simulations using the leapfrog integration algorithm," J. Chem. Phys. **127**, 184102 (2007).
[76]S. Nosé, "A molecular dynamics method for simulations in the canonical ensemble," Mol. Phys. **52**, 255–268 (1984).
[77]W. G. Hoover, "Canonical dynamics: Equilibrium phase-space distributions," Phys. Rev. A **31**, 1695 (1985).
[78]M. Parrinello and A. Rahman, "Polymorphic transitions in single crystals: A new molecular dynamics method," J. Appl. Phys. **52**, 7182–7190 (1981).
[79]U. Essmann, L. Perera, M. L. Berkowitz, T. Darden, H. Lee, and L. G. Pedersen, "A smooth particle mesh Ewald method," J. Chem. Phys. **103**, 8577–8593 (1995).
[80]J. L. F. Abascal, E. Sanz, R. García Fernández, and C. Vega, "A potential model for the study of ices and amorphous water: TIP4P/Ice," J. Chem. Phys. **122**, 234511 (2005).
[81]J. J. Potoff and J. I. Siepmann, "Vapor–liquid equilibria of mixtures containing alkanes, carbon dioxide, and nitrogen," AIChE J. **47**, 1676–1682 (2001).
[82]M. M. Conde and C. Vega, "Note: A simple correlation to locate the three phase coexistence line in methane-hydrate simulations," J. Chem. Phys. **138**, 056101 (2013).
[83]J. M. Míguez, M. M. Conde, J.-P. Torré, F. J. Blas, M. M. Piñeiro, and C. Vega, "Molecular dynamics simulation of $CO_2$ hydrates: Prediction of three phase coexistence line," J. Chem. Phys. **142**, 124505 (2015).
[84]J. Algaba, E. Acuña, J. M. Míguez, B. Mendiboure, I. M. Zerón, and F. J. Blas, "Simulation of the carbon dioxide hydrate-water interfacial energy," J. Colloid Interface Sci. **623**, 354–367 (2022).
[85]I. M. Zerón, J. M. Míguez, B. Mendiboure, J. Algaba, and F. J. Blas, "Simulation of the $CO_2$ hydrate–water interfacial energy: The mold integration–guest methodology," J. Chem. Phys. **157**, 134709 (2022).
[86]C. Romero-Guzmán, I. M. Zerón, J. Algaba, B. Mendiboure, J. M. Míguez, and F. J. Blas, "Effect of pressure on the carbon dioxide hydrate–water interfacial free energy along its dissociation line," J. Chem. Phys. **158**, 194704 (2023).
[87]H. Tanaka, T. Yagasaki, and M. Matsumoto, "On the phase behaviors of hydrocarbon and noble gas clathrate hydrates: Dissociation pressures, phase diagram, occupancies, and equilibrium with aqueous solution," J. Chem. Phys. **149**, 074502 (2018).
[88]V. Buch, P. Sandler, and J. Sadlej, "Simulations of $H_2O$ solid, liquid, and clusters, with an emphasis on ferroelectric ordering transition in hexagonal ice," J. Phys. Chem. B **102**, 8641–8653 (1998).
[89]J. H. Weijs, J. R. T. Seddon, and D. Lohse, "Diffusive shielding stabilizes bulk nanobubble clusters," ChemPhysChem **13**, 2197–2204 (2012).
[90]W. Lechner and C. Dellago, "Accurate determination of crystal structures based on averaged local bond order parameters," J. Chem. Phys. **129**, 114707 (2008).
[91]I. M. Zerón, J. Algaba, J. M. Míguez, B. Mendiboure, and F. J. Blas, "Rotationally invariant local bond order parameters for accurate determination of hydrate structures," Mol. Phys. **122** e2395438 (2024).
[92]J. Wedekind, R. Strey, and D. Reguera, "New method to analyze simulations of activated processes," J. Chem. Phys. **126**, 134103 (2007).
[93]G. Chkonia, J. Wölk, R. Strey, J. Wedekind, and D. Reguera, "Evaluating nucleation rates in direct simulations," J. Chem. Phys. **130**, 064505 (2009).

[94]Z. Xu and Y. Konno, "Morphological change of hydrate caused by Ostwald ripening and sintering," Energy Fuels **39**, 4238–4248 (2025).
[95]S. Blazquez, M. M Conde, C. Vega, and E. Sanz, "Growth rate of $CO_2$ and $CH_4$ hydrates by means of molecular dynamics simulations," J. Chem. Phys. **159**, 064503 (2023).
[96]G.-J. Guo, Y.-G. Zhang, C.-J. Liu, and K.-H. Li, "Using the face-saturated incomplete cage analysis to quantify the cage compositions and cage linking structures of amorphous phase hydrates," Phys. Chem. Chem. Phys. **13**, 12048–12057 (2011).
[97]Z. Zhang, M. R. Walsh, and G.-J. Guo, "Microcanonical molecular simulations of methane hydrate nucleation and growth: Evidence that direct nucleation to Si hydrate is among the multiple nucleation pathways," Phys. Chem. Chem. Phys. **17**, 8870–8876 (2015).
[98]L. C. Jacobson and V. Molinero, "Can amorphous nuclei grow crystalline clathrates? The size and crystallinity of critical clathrate nuclei," J. Am. Chem. Soc. **133**, 6458–6463 (2011).
[99]G.-J. Guo and Z. Zhang, "Open questions on methane hydrate nucleation," Commun. Chem. **4**, 102 (2021).
[100]P. Montero de Hijes, J. R. Espinosa, E. Sanz, and C. Vega, "Interfacial free energy of a liquid-solid interface: Its change with curvature," J. Chem. Phys. **151**, 144501 (2019).
[101]M. M. Conde, C. Vega, G. A. Tribello, and B. Slater, "The phase diagram of water at negative pressures: Virtual ices," J. Chem. Phys. **131**, 034510 (2009).
[102]J. R. Espinosa, C. Vega, and E. Sanz, "The mold integration method for the calculation of the crystal-fluid interfacial free energy from simulations," J. Chem. Phys. **141**, 134709 (2014).
[103]J. R. Espinosa, C. Vega, and E. Sanz, "Ice–water interfacial free energy for the TIP4P, TIP4P/2005, TIP4P/ice, and mW models as obtained from the mold integration technique," J. Phys. Chem. C **120**, 8068–8075 (2016).
[104]D. Kashchiev and A. Firoozabadi, "Nucleation of gas hydrates," J. Cryst. Growth **243**, 476–489 (2002).
[105]J. R. Espinosa, C. Vega, and E. Sanz, "Homogeneous ice nucleation rate in water droplets," J. Phys. Chem. C **122**, 22892–22896 (2018).
[106]M. T. J. Barwood, P. J. Metaxas, V. W. S. Lim, C. C. Sampson, M. L. Johns, Z. M. Aman, and E. F. May, "Extracting nucleation rates from ramped temperature measurements of gas hydrate formation," Chem. Eng. J. **450**, 137895 (2022).
[107]P. J. Metaxas, V. W. S. Lim, C. Booth, J. Zhen, P. L. Stanwix, M. L. Johns, Z. M. Aman, G. Haandrikman, D. Crosby, and E. F. May, "Gas hydrate formation probability distributions: Induction times, rates of nucleation and growth," Fuel **252**, 448–457 (2019).
[108]N. Maeda, "Nucleation curves of model natural gas hydrates on a quasi-free water droplet," AIChE J. **61**, 2611–2617 (2015).
[109]P. Warrier, M. N. Khan, V. Srivastava, C. M. Maupin, and C. A. Koh, "Overview: Nucleation of clathrate hydrates," J. Chem. Phys. **145**, 211705 (2016).
[110]J. R. Espinosa, C. Vega, C. Valeriani, D. Frenkel, and E. Sanz, "Heterogeneous versus homogeneous crystal nucleation of hard spheres," Soft Matter **15**, 9625–9631 (2019).
[111]V. Bianco, P. M. de Hijes, C. P. Lamas, E. Sanz, and C. Vega, "Anomalous behavior in the nucleation of ice at negative pressures," Phys. Rev. Lett. **126**, 015704 (2021).
[112]T. Uchida, T. Ebinuma, and T. Ishizaki, "Dissociation condition measurements of methane hydrate in confined small pores of porous glass," J. Phys. Chem. B **103**, 3659–3662 (1999).
[113]T. Uchida, T. Ebinuma, S. Takeya, J. Nagao, and H. Narita, "Effects of pore sizes on dissociation temperatures and pressures of methane, carbon dioxide, and propane hydrates in porous media," J. Phys. Chem. B **106**, 820–826 (2002).
[114]R. Anderson, M. Llamedo, B. Tohidi, and R. W. Burgass, "Characteristics of clathrate hydrate equilibria in mesopores and interpretation of experimental data," J. Phys. Chem. B **107**, 3500–3506 (2003).
[115]R. Anderson, M. Llamedo, B. Tohidi, and R. W. Burgass, "Experimental measurement of methane and carbon dioxide clathrate hydrate equilibria in mesoporous silica," J. Phys. Chem. B **107**, 3507–3514 (2003).